Journal of Materials Chemistry B

ROYAL SOCIETY OF CHEMISTRY

PAPER

View Article Online
View Journal | View Issue

Cite this: J. Mater. Chem. B, 2026, 14, 354

Smart antimicrobial wound dressings based on mechanically and biologically tuneable hybrid films

Sara Sadati,[ab] Marcus J Swann,[c] Rui Chen,[c] Jérôme Charmet,[bde] Meera Unnikrishnan,[b] Steven L Percival[c] and Dmitry Isakov *[a]

Received 23rd September 2025,
Accepted 22nd November 2025

DOI: 10.1039/d5tb02157j

rsc.li/materials-b

Chronic wounds remain a major clinical burden, often complicated by infections sustained within antibiotic-resistant biofilms. Smart wound dressings that combine structural support with controlled antimicrobial release are emerging as a powerful strategy to address these challenges. Among the biomaterial platforms, gelatin offers excellent biocompatibility, biodegradability, and chemical versatility, but its poor mechanical strength limits its standalone use. In this work, we present crosslinked gelatin–PEO (GG:PEO) hybrid films, stabilized with glycidoxypropyltrimethoxysilane (GPTMS), as a versatile platform for responsive wound management. By tuning the gelatin/PEO ratio, the films achieved up to a 57% increase in flexibility compared to pristine gelatin while retaining structural integrity. Antimicrobial functionality was conferred through incorporation of a novel multifunctional metal complex (MMC) comprising EDTA-chelated silver and copper ions. Crucially, the GG:PEO composition enabled modulation of drug release kinetics, providing a means to fine-tune bacterial inhibition. Optimized films suppressed bacterial growth and metabolism, with disc diffusion assays showing up to a 68% increase in inhibition zones at higher PEO ratios. Together, these findings demonstrate a robust and adaptable biomaterial system where both mechanical and antimicrobial properties can be engineered on demand. Such tunable composite films hold promise not only for advanced wound dressings but also for wider biomedical applications, including implant coatings and infection-responsive therapeutic devices.

1. Introduction

Biofilms, surface-attached microbial communities embedded in extracellular matrices, pose a great challenge in wound care. Biofilms are reported to be up to a thousand times more tolerant to antibiotics due to many contributing factors including the extracellular matrix, which can act like a protective layer against drug entry.[1,2] Chronic wounds and the underlying pathology predispose a patient to the growth of biofilms and therefore persistent and reoccurring microbial infections. This situation exacerbates the burden of antimicrobial resistance and emphasises the need for advanced therapies that can both detect early signs of infection and respond with targeted treatment. Biomaterials with on-demand or sustained smart antibiofilm release can help minimise these infections and promote faster healing.[3–5]

For the material matrix of such a smart dressing, gelatin is an attractive biopolymer. Gelatin, a protein derived from collagen, is extensively used in biomedical applications owing to its intrinsic biodegradability, biocompatibility, and amenability to chemical functionalisation.[6] The ability of gelatin to be functionalised with biomolecules and therapeutic agents further enhances its versatility, enabling its use in wound healing, drug delivery, and tissue engineering, where it can provide controlled release. In addition, gelatin is gaining interest in developing biomaterial platforms that offer antimicrobial release capabilities.[7–11]

While gelatin holds favorable biological properties, it is a water-soluble protein obtained through the partial hydrolysis of collagen. Therefore, its denaturation and weak mechanical strength often limit its use in biological environments. To address this, crosslinking is typically employed to enhance the mechanical stability of gelatin in aqueous media. Several chemical (*e.g.*, glutaraldehyde,[12] genipin,[13,14] carbodiimides[15]) and physical (*e.g.*, plasma treatment,[16] photocrosslinking[17]) crosslinkers have been used to tailor the properties of gelatin

[a] WMG, University of Warwick, Coventry, UK. E-mail: d.isakov@warwick.ac.uk
[b] Division of Biomedical Sciences, Warwick Medical School, University of Warwick, Coventry, UK
[c] 5D Health Protection Group, Accelerator Building, 1 Daulby Street, Liverpool, UK
[d] University of Bern, Bern, Switzerland
[e] HE-Arc Ingenierie, HES-SO University of Applied Sciences and Art of Western Switzerland, 2000, Neuchatel, Switzerland

for biomedical applications. However, many of the available crosslinkers are associated with potential cytotoxicity, longer processing times, or in the case of physical crosslinkers, temporary crosslinking.[18–20] Glycidoxypropyltrimethoxysilane (GPTMS) offers a promising alternative for crosslinking gelatin, addressing many of the issues associated with conventional crosslinkers. GPTMS is an organosilane that reacts with gelatin through its epoxy group while undergoing hydrolysis and condensation reactions to form siloxane bonds.[21] This dual functionality provides *in situ* crosslinking, enhances the mechanical properties and stability of gelatin, and avoids the cytotoxicity concerns linked to chemical crosslinkers such as glutaraldehyde.[22,23] Additionally, GPTMS crosslinking occurs under mild conditions, which allows it to be used in processes to encapsulate and release bioactive molecules.[24]

However, crosslinked gelatin often exhibits high brittleness, difficult processability, and limited porosity. These issues are typically addressed by blending them with other compatible polymers and reducing interchain interactions.[25,26] A potential candidate is polyethylene oxide (PEO), a water-soluble biocompatible synthetic polymer that is widely used in pharmaceuticals and medical applications due to its tunable properties over a wide range of molecular weights.[27] PEO is also known for its hydrophilicity and flexibility, which, when combined with gelatin, can improve the elasticity and swelling behavior of the resulting hydrogel.

To confer antimicrobial activity to gelatin-based scaffolds and other hydrogels, various antimicrobial/antibiofilm agents can be incorporated directly into the films.[28] Although the mechanism behind the activity of metal-based compounds, *e.g.*, silver and copper, in killing microbes and disrupting biofilms is not yet fully understood, their effectiveness is mostly associated with water solubility and stability, redox ability, and rate of ionic release. Therefore, silver and copper are widely employed in wound care materials owing to their broad-spectrum antimicrobial efficacy and low risk of resistance development.[29] Reported cytotoxic thresholds for mammalian skin cells are typically higher than the concentrations required for antibacterial action, allowing an appropriate therapeutic window when release is controlled.[30–32] Despite demonstrating broad-spectrum antimicrobial activity in the numerous research studies however, silver complexes have limited functionality *in vivo* due to the rapid clearance and uncontrolled release rates and delivery at sub-therapeutic levels.[33,34] To overcome this issue, biodegradable materials such as crosslinked gelatin–PEO hybrids could be used to integrate these active antibiofilm/antimicrobial compounds into their network and promote a more stable and localized delivery.

Despite progress in antimicrobial biomaterials, current approaches typically offer fixed release profiles that cannot be adjusted to match infection severity or wound healing stages. Furthermore, most studies focus on single-parameter optimization (*e.g.*, antimicrobial concentration alone) without addressing the interplay between material properties and antimicrobial delivery.[35] There remains an unmet need for platforms enabling independent control over initial bacterial inhibition *versus* sustained suppression through rational material design.

In this work, we present a novel biomaterial platform based on crosslinked gelatin–polyethylene oxide (GG:PEO) hybrid films functionalised with an antibiofilm multifunctional metal complex (MMC) comprising silver and copper chelated with EDTA, designed to exploit the complementary mechanisms of both metals (Fig. 1). By incorporating more than one active metal species, we introduce dual-metal complex that have potential synergistic and increased antibacterial effects, as each ion operates through distinct mechanisms.[36] Our approach integrates the biodegradability and biocompatibility of gelatin with the hydrophilicity and flexibility of PEO, offering controlled modulation of swelling behavior, dissolution rates, and mechanical robustness. The incorporation of the MMC as an antibacterial additive to the crosslinked hybrid films

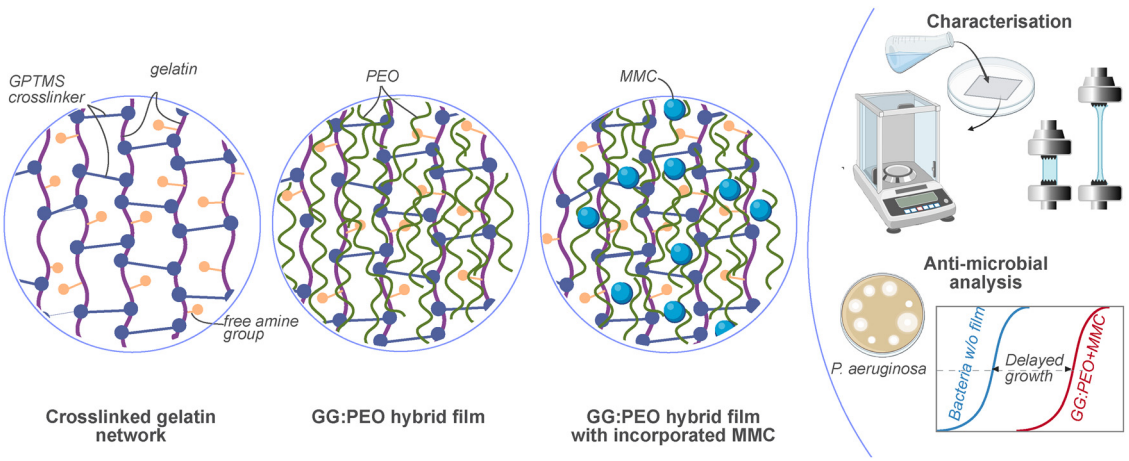

Fig. 1 Schematic illustration of the GG:PEO film preparation and characterisation. MMC integrated films were prepared in three steps. First, gelatin was crosslinked using GPTMS reagent. GG:PEO hybrid films were then prepared by blending the crosslinked gelatin solution with PEO. MMC particles were incorporated in the final step and were allowed to dry out completely. Physicochemical and mechanical properties of GG:PEO films were studied. Antimicrobial analysis of the MMC incorporated films were performed against *P. aeruginosa*.

demonstrates antimicrobial functionality and controlled release kinetics. This integration of a stable, dual-metal antimicrobial complex within a mechanically tunable hybrid matrix provides a new route to design smart wound dressings capable of on-demand antimicrobial release. To our knowledge, this is the first demonstration of a GPTMS-crosslinked gelatin–PEO platform that allows independent tuning of both structural and antimicrobial performance, paving the way for responsive, infection-targeted biomaterials for wound healing and implant applications.

2. Experimental

2.1. Materials

Gelatin powder from porcine skin (type A, 300 bloom, 70–90% biuret) and 3-glycidyloxypropyltrimethoxysilane (GPTMS, ≥98%) were purchased from Sigma-Aldrich. Polyethylene oxide (PEO), M.W. 300 000 was obtained from Alpha Aesar. Mixed metal complex (MMC) was prepared by 5D health protection group (5D patent protected – US20190133131A1).[37] Ninhydrin reagent (2% solution) was purchased from Merck. Resazurin sodium salt (dye content ≥80%) was obtained from Acros Organics. Luria-Bertani (LB) broth and tryptic soy broth (TSB) were obtained from Merck Millipore. All materials used were of reagent grade and were used without any further purification.

2.2. Crosslinking gelatin with GPTMS

5% w/v gelatin solution was prepared by adding gelatin powder to Milli-Q water at 50 °C and stirring until fully dissolved. GPTMS was added to the gelatin solution and mixed for an hour at 50 °C to initiate the epoxy-amine curing reaction[38] and to allow GPTMS and gelatin to conjugate. Crosslinked gelatin solution was cast into Petri dishes (inner diameter 86 mm). The cast gels were air-dried at room temperature for varying durations (12 h–72 h) prior to characterisation tests.

GPTMS to gelatin ratio amounts were calculated and tested based on the molar concentration of amino groups present in the hydroxylysine, lysine, and arginine residues of gelatin. 92 μL GPTMS per gram gelatin (~1 : 10 w/w) was previously suggested for optimal cell proliferation on electrospun nanofibers.[22] In this work, a range of GPTMS to gelatin ratios around the suggested ratio were tested for films in aqueous environments. Films with lower ratios did not survive after overnight immersion in blank nutrient media (data not included), thus only higher ratios were considered.

For clarity, hereafter we denote and use the mass ratios between GPTMS and gelatin (*i.e.* 1 : 10 w/w, 1.5 : 10 w/w, 2 : 10 w/w, and 3 : 10 w/w) based on the density of GPTMS. GPTMS-crosslinked gelatin films will hereafter be referred to as GG throughout the text. This notation reflects the mass ratio of GPTMS to gelatin, where the volume of 92 μL of GPTMS (ρ = 1.07 g mL^{-1}) equates to approximately 100 mg. Table 1 summarizes the volumes and molar ratios between gelatin and GPTMS.

Table 1 Summary of GPTMS content in crosslinked gelatin films. Shaded column indicates the selected notation in this work

GPTMS to gelatin mass ratio	GPTMS volume per gelatin gram (μL)	GPTMS to gelatin amino groups molar ratio
1 : 10	92	1 : 2
1.5 : 10	138	1.5 : 2
2 : 10	184	1 : 1

2.3. Preparation of GPTMS–gelatin–PEO hybrid films

GPTMS/gelatin/PEO (GG:PEO) films were prepared by blending the GG solution with an aqueous PEO solution. Similar to the previous section, a 10% w/v gelatin solution was prepared and functionalised with varying amounts of GPTMS (1 : 10–3 : 10 w/w). Separately, a 10% w/v PEO stock solution was prepared by dissolving PEO in Milli-Q water under constant stirring for 6–8 hours at 80 °C.

To prepare GG:PEO hybrid films with a final 5% v/w gelatin concentration and varying PEO concentrations (1–4% v/w), the 10% w/v functionalised gelatin and PEO stock solutions were diluted and mixed in appropriate ratios. The mixtures were stirred at 50 °C for at least one hour for homogeneity. The resulting blends designated as GG:PEO1%, GG:PEO2%, GG:PEO3%, and GG:PEO4%, corresponding to 1%–4% w/v PEO concentrations, were then cast into films by spreading each blend into Petri dishes and air-drying for 24–48 h.

The PEO concentrations investigated here (1–4% w/v) were chosen purposefully to keep gelatin as the dominant, GPTMS-crosslinked matrix while allowing progressive modulation of hydrophilicity, swelling and release by increasing PEO content. Lower PEO loadings (<1% w/v) are expected to behave similarly to GG (no PEO) and therefore were not informative for release tuning. Conversely, substantially higher PEO loadings (>4% w/v) were avoided because PEO is highly water-soluble and preliminary trials showed that very high PEO content causes rapid PEO dissolution and loss of mechanical integrity in aqueous environments (see swelling/dissolution data in Results). Thus, the 1–4% w/v window provides a practical balance between preserving the crosslinked gelatin network and enabling controlled increases in swelling and diffusion-mediated release.

For MMC incorporated GG:PEO films, 2% w/w MMC films contained 10 mg MMC in 500 mg GGPEO cast films. Dried films with 10 mm diameter were cut for Kirby-Bauer tests. Samples with varying MMC concentrations (100, 300, 1000 ppm) were similarly prepared for resazurin viability assay.

2.4. Determination of degree of crosslinking *via* ninhydrin assay

A ninhydrin assay was used to quantify the degree of gelatin crosslinking in GG and GG:PEO films. Ninhydrin (2,2-dihydroxyindane-1,3-dione) reacts with the free amino groups to produce a colored compound known as Ruhemann's purple. The intensity of the resulting color is directly proportional to the concentration of amino acids in the sample, allowing for their quantification through spectrophotometric measurement

at wavelengths around 570 nm.[39,40] Crosslinked gelatin films with different crosslinker percentages and dried for different periods of time were tested. Crosslinking extent was also measured in GG:PEO films with varying concentrations of PEO and dried for different periods of time. A precise amount of sample (10 ± 0.5 mg) was heated with 0.5 ml ninhydrin solution for exactly 10 min in a water bath at 80 °C. A 2% reagent with ninhydrin and hydrindantin in DMSO and lithium acetate buffer (pH 5.2) was used for better color yield and stability. Subsequently, 500 μL of absolute ethanol was mixed with 10 μL of each sample. Ethanol-to-sample volume ratio was optimized and selected out of a range of volume ratios based on the linear response of absorbance over gelatin concentration. Absorbance was recorded on a spectrophotometer (FLUOstar Omega) at the 570 nm wavelength with pure gelatin as a reference. Linear regression was performed with a correlation of 0.9994. Free amino groups were normalized according to gelatin content in GG:PEO samples. The extent of crosslinking was defined as:

$$\text{Crosslinking degree (\%)} = \frac{NH_0 - NH_t}{NH_0} \times 100\%, \quad (1)$$

where NH_0 is the amount of free amino groups in uncrosslinked gelatin and NH_t is the amount of free amino groups in gelatin after crosslinking.[41]

2.5. Physico-chemical characterisations

2.5.1. Fourier transform infrared-attenuated total reflectance spectroscopy (FTIR-ATR). Chemical analysis of GG and GG:PEO films was performed by ATR-FTIR spectroscopy over a range of 4000 cm^{-1}–500 cm^{-1} with 4 cm^{-1} resolution and 32 scans using Bruker Tensor 27 FTIR spectrometer.

2.5.2. Contact angle measurements. The static water contact angle (WCA) for gelatin, GG, and GG:PEO1%–4% films was measured on their respective cast films using Microqubic MRCL700 3D Imager Pro at room temperature. 5 μL droplet of distilled water was added on each sample and contact angle measurements were conducted using drop analysis plugin on ImageJ. Each reported angle represents the average of at least five measurements taken at different points on the surface. Results are presented as the mean static contact angle ± standard deviation.

2.5.3. Swelling and dissolution studies. Swelling and dissolution rates of GG:PEO films were measured in the presence of phosphate buffered saline (PBS). Solvent-cast films were air-dried for 48 h prior to weighing. Samples were immersed in sterile PBS (0.01 M, pH 7.4) and were allowed to incubate for 24 h at 37 °C. After 24 h, remaining liquid was removed and the films were squeezed between filter papers to remove any excess water from the films. Samples were weighed again to assess the swelling degree and were incubated at 37 °C for another 24 h to dry out prior to weighting. Swelling and dissolution degrees were calculated as:

$$\text{Swelling degree (\%)} = \frac{W_{\text{swollen}} - W_{\text{dry}}}{W_{\text{dry}}} \times 100\%, \quad (2)$$

where W_{swollen} is the weight of wet samples, and W_{dry} is the weight of dried samples.

$$\text{Degree of dissolution (\%)} = \frac{W_{\text{initial}} - W_{\text{dry}}}{W_{\text{initial}}} \times 100\%, \quad (3)$$

where W_{initial} is the initial weight, and W_{dry} is the weight of dried samples after testing.

2.5.4. Gelatin leaching (UV absorption). Concentration of gelatin leaching from GG:PEO films in an aqueous environment was quantified using NanoDrop One Spectrophotometer (ThermoFisher). Beer–Lambert law typically allows for the direct calculation of concentration from absorbance using a known extinction coefficient.[42,43] Gelatin, being a complex biopolymer, does not have a well-defined or consistent extinction coefficient.[44] Therefore, a standard curve was generated by serially diluting gelatin solutions. Linear regression was performed with a correlation of 0.9966 (205 nm).

GG:PEO samples were air-dried for 48 h and were incubated for 24 h at 37 °C in the presence of 20 ml sterile 0.01 M PBS. After 24 h, the immersion medium was taken and further diluted for absorbance measurements. 1.5 μL of diluted solutions was placed on the pedestal, and measurements were taken in triplicates.

2.6. Mechanical characterisation

Tensile strength and Young's modulus of GG:PEO films were measured using a 3367 30 kN static tester (Instron, UK) with a 500 N load cell, a cross-head speed of 1 mm min^{-1}, and a break limit of 40%. Rectangular films with 40 mm length and 25 mm width were tested by fixing the ends of each sample with adhesive tape to strengthen the clamping grip (35 mm gauge length). Young's modulus was automatically calculated using the slope on the initial linear portion of stress–strain curves using least squares fit. Tensile strength σ and strain ε at break were calculated according to eqn (4) and (5), respectively:

$$\sigma(\text{MPa}) = \frac{F}{A}, \quad (4)$$

$$\varepsilon = \frac{\Delta L}{L_0} \times 100\%, \quad (5)$$

where F is the breaking force, A is the cross-sectional area of the sample, ΔL is the displacement (extension) at the breaking point, and L_0 is the initial sample length. At least four replicates were performed for each sample group. Results were expressed as an average value ± standard deviation.

Toughness (absorbed energy to failure) was computed as the numerical integral of the stress–strain curves up to the point of fracture using the trapezoidal rule:

$$\text{Toughness} = \int_0^{\varepsilon_{\max}} \sigma(\varepsilon)\mathrm{d}\varepsilon, \quad (6)$$

where $\varepsilon_{\max}$ is defined as the last data point before complete rupture of the film, where stress dropped to zero. For samples that exhibited gradual yielding rather than abrupt fracture, integration was performed up to the final recorded strain point while the specimen remained continuous and under load.

2.7. Scanning electron microscopy (SEM)

The surface morphology of the MMC incorporated films was examined using a TM3030Plus tabletop scanning electron microscope (Hitachi, Japan). Samples were mounted on aluminum stubs using double-sided conductive carbon tape and imaged under an accelerating voltage of 15 kV. Micrographs were captured at various magnifications to analyze surface topography and structural characteristics.

Elemental analysis was performed using the integrated energy-dispersive X-ray spectroscopy (EDS) detector. Spectra were collected from selected areas of the samples to identify and confirm the presence of key elements, particularly those associated with the MMC components. AZtec software (Oxford Instruments) was used for spectrum acquisition, qualitative analysis, and elemental mapping.

2.8. Antibacterial studies

Antibacterial activities of MMC-incorporated GG:PEO films were investigated against one of the most prevalent wound opportunistic pathogens, the Gram-negative bacterium *P. aeruginosa* PA14.

Bacterial glycerol stocks were cultured overnight on Luria-Bertani (LB) agar. A single colony was picked and inoculated in LB liquid medium. Working bacteria cultures were prepared by incubating overnight at 37 °C, 180 rpm to an optical density (OD_{600}) of 1.0 which corresponded to a microbial count of 8×10^8 CFU per mL. Fresh bacterial cultures were prepared from a different colony for each experiment.

For the Kirby-Bauer disc diffusion test, 2% w/w MMC incorporated GG:PEO films with the same size (10 mm diameter) and thickness (approx. 60 μm) were prepared. We defined the positive control to be the bacterial testing of GG:PEO films with no MMC and the negative control to be the GG:PEO films in the blank medium with no bacteria. All the samples were UV-sterilized at 254 nm for 10 min prior to experiments. 400 μL of the bacterial cultures were evenly spread on tryptic soy agar plates. Next, sterilized films were carefully placed on the plates and were incubated at 37 °C for 24 h. The zone of inhibition (ZOI) was measured with ±0.5 mm accuracy and averaged over 5 replicates for each GG:PEO composition.

Resazurin viability assay was used to investigate the effect of GG:PEO film composition on release profiles over time. MMC concentration for each strain was optimized to monitor the concentration series in which the highest effect in growth profiles was observed. Resazurin viability assay was conducted as described previously.[45] Briefly, a stock solution of resazurin dye was prepared by dissolving 0.05 g of resazurin powder in 10 mL of sterile 1× PBS. Sterilized films (10 mm diameter) were placed in each well in a 48-well plate. A final concentration of 25 μg mL^{-1} resazurin was added to each well in a sterile 48-well plate. Bacterial cultures corresponding to the initial 0.05 OD_{600} were introduced to each well using LB media, reaching a total volume of 1 mL in each well. GG:PEO films with no MMC in the bacteria culture were tested as positive control, while GG:PEO films with no MMC in blank nutrient media were used as negative control. The plate was incubated at 37 °C in a BMG Labtech FLUOstar Omega plate reader and fluorescence measurements at 544 nm/610 nm excitation/emission wavelengths were measured every minute for 24 h. Three independent experiments (on three different days) were performed with three technical replicates per experiment. The average ± standard deviation of the three biological replicates were reported.

Quantitative determination of silver release from MMC-incorporated GG:PEO films was performed using anodic stripping amperommetry assay based on the protocol described by Swann *et al.*[46] Screen-printed gold electrodes were used for all measurements. Measurements were performed using a controlled potential sequence as follows (Metrohm Autolab PGSTAT128N): an initial deposition step at −0.2 V for 50 seconds, followed by sequential potential steps at −0.05 V, 0 V, 0.05 V, 0.1 V, and 0.15 V (each held for 5 seconds), and finally 0.2 V for 100 seconds. The charge passed during the 0.1 V step was used for quantitative analysis as it demonstrated the highest linearity with MMC concentration. Each measurement was performed in triplicate to ensure reproducibility. Calibration curves were generated using MMC standard solutions to establish a linear relationship between anodic stripping charge and concentration. For release studies, GG:PEO2% films (~1 cm diameter, ~65 μm thickness, average 6.8 mg weight) loaded with 1% w/w MMC were immersed in 500 μL LB medium at 37 °C. At each sampling point (0–24 h), the supernatant was collected, analysed immediately, and replaced with fresh medium. Silver concentrations (μg mL^{-1}) were converted to absolute released mass (μg) based on solution volume, and normalised to film surface area (0.785 cm^2). From these values, both cumulative release and release fluxes were calculated. Cumulative average flux (μg cm^{-2} h^{-1}) was determined as the total silver released up to each time point, divided by the elapsed time and surface area.

2.9. Statistical analysis

Statistical analysis was conducted using GraphPad Prism 10. Data were analyzed and compared using analysis of variance (ANOVA). Multiple comparisons were made among groups using Tukey's multiple comparison tests. Standard curves were generated, and 95% confidence intervals were calculated for the fitted lines. All tests were performed in triplicates, and results were expressed as average value ± standard deviation. A value of $^*P \leq 0.05$ was considered statistically significant.

3. Results and discussions

3.1. Infrared analysis of crosslinked gelatin films

To investigate the chemical interactions in GPTMS-crosslinked gelatin films, FTIR spectroscopy was employed. Fig. 2 illustrates the chemical mechanism for crosslinking gelatin with GPTMS. The process follows a two-step mechanism: in the first, GPTMS reacts with the amine groups in gelatin, opening the oxirane ring and forming a covalent bond with the polypeptide chains. Simultaneously, the trimethoxy groups of GPTMS hydrolyze in

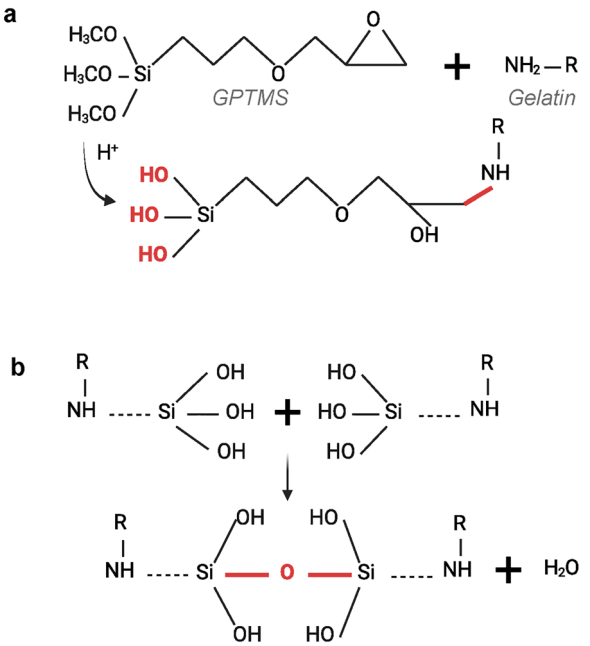

Fig. 2 Two-step mechanism of crosslinking gelatin with GPTMS. (a) The methoxy groups (–OCH_3) on GPTMS are hydrolyzed, forming silanol groups (–SiOH). At the same time, GPTMS also interacts with the nucleophilic amino groups (–NH_2) present on the lysine residues of gelatin. (b) In the second phase, the formed silanol groups on GPTMS undergo a condensation reaction, leading to the formation of siloxane (Si–O–Si) bonds. These siloxane linkages create a stable inorganic network that interconnects the gelatin chains, resulting in a three-dimensional structure.

water, forming pendant silanol groups (Si–OH) at the other end of GPTMS molecules. Full crosslinking occurs in the second step, where these silanol groups condense to form siloxane (Si–O–Si) bonds.[22,47]

The FTIR spectra presented in Fig. 3a provide insight into the interactions between gelatin and GPTMS in solvent-casted films. Characteristic absorption bands for gelatin were observed in both crosslinked and uncrosslinked gelatin films at 1632 cm^{-1} (amide I, C=O stretching), 1545 cm^{-1} (amide II, N–H bending), and 1240 cm^{-1} (amide III, C–N stretching).[48–50] Additionally, a peak at 910–920 cm^{-1} appeared in crosslinked samples, corresponding to the hydrolysis of trimethoxy groups and the formation of silanol groups. The shoulder around 1100 cm^{-1} was attributed to Si–O–Si bonds, indicating successful crosslinking by condensation. These characteristic peaks directly confirmed the incorporation of GPTMS into the gelatin network.

The spectra in Fig. 3b revealed that increasing GPTMS concentrations led to a sharper and more prominent silanol peak (910–920 cm^{-1}), indicating a higher degree of crosslinking. Additionally, the siloxane band around 1100 cm^{-1}, which broadened with higher GPTMS levels, can be attributed to the formation of more extended or branched Si–O–Si conjugates, as suggested by Launer *et al.*[51]

The effect of GPTMS concentration on chemical composition was further investigated in the presence of PEO (1 : 1 w/w PEO/gelatin). PEO exhibits several characteristic bands similar to those of proteins and organosilane agents.[52,53] In Fig. 3c, overlapping peaks were observed at ~1100 cm^{-1} corresponding to both siloxane bonds in crosslinked gelatin chains and C–O–C stretching vibrations in PEO.

This overlap complicates the interpretation, as the siloxane peak, which is an indicator of successful crosslinking, is superimposed with the PEO-specific C–O–C stretching. However, the incorporation of active silanol groups in samples with higher GPTMS concentrations was confirmed by the sharp and prominent peaks at 910–920 cm^{-1}, which remain distinct and unaffected by PEO. The less prominent silanol characteristic band at the lower GPTMS concentrations suggests potential consumption of silanol groups by PEO ether groups, likely through hydrogen bonding.[54]

3.2. Quantification of gelatin crosslinking and optimisation of GG molar ratio

The extent of gelatin crosslinking was quantified using ninhydrin assay by measuring the free alpha-amino groups in the samples. Both crosslinking duration and concentration have been previously suggested to significantly influence the crosslinking levels.[55] To investigate these effects, solvent-casting films with varying molar ratios of GPTMS to gelatin were evaluated after air-drying for different periods. As shown in Fig. 4a, the silane epoxy groups effectively crosslinked the gelatin chains by reacting with the amine groups. A clear increasing trend in crosslinking degrees was observed with higher crosslinker concentrations and extended drying periods. This suggests that the crosslinking degree, and consequently the properties of the obtained membranes can be finely tuned by adjusting the amount of crosslinker and the drying time.

Greater variability was observed in samples crosslinked with lower GPTMS amounts and shorter drying periods, likely due to incomplete crosslinking. Shorter drying times might lead to more extensive crosslinking at the surface compared to the bulk, likely caused by different evaporation rates.[56] The maximum crosslinking extent, 68.1% ± 6.2, was reached after 72 h of air-drying in samples with a 2 : 10 mass ratio of GPTMS to gelatin amine groups. Increasing the GPTMS concentration beyond this ratio did not significantly affect the degree of crosslinking after 72 h, suggesting that a plateau is reached once condensation is complete. Since the availability of the free amino groups in the gelatin molecules is limited, the maximum degree of crosslinking remains constant regardless of further increase in GPTMS volume.[57,58]

Based on the FTIR spectra and crosslinking degrees, and to ensure that enough silanol groups were present in the solution to be conjugated by gelatin chains, we selected the 2 : 10 mass ratio between GPTMS and gelatin (*i.e.* 184 μL per gram of gelatin) for the following experiments which is referred as GG:PEO0%.

To determine whether PEO influences gelatin crosslinking by GPTMS, we measured the degree of crosslinking in GG:PEO films with varying concentrations and drying times (Fig. 4b). Although samples with a similar weight were cut and analyzed

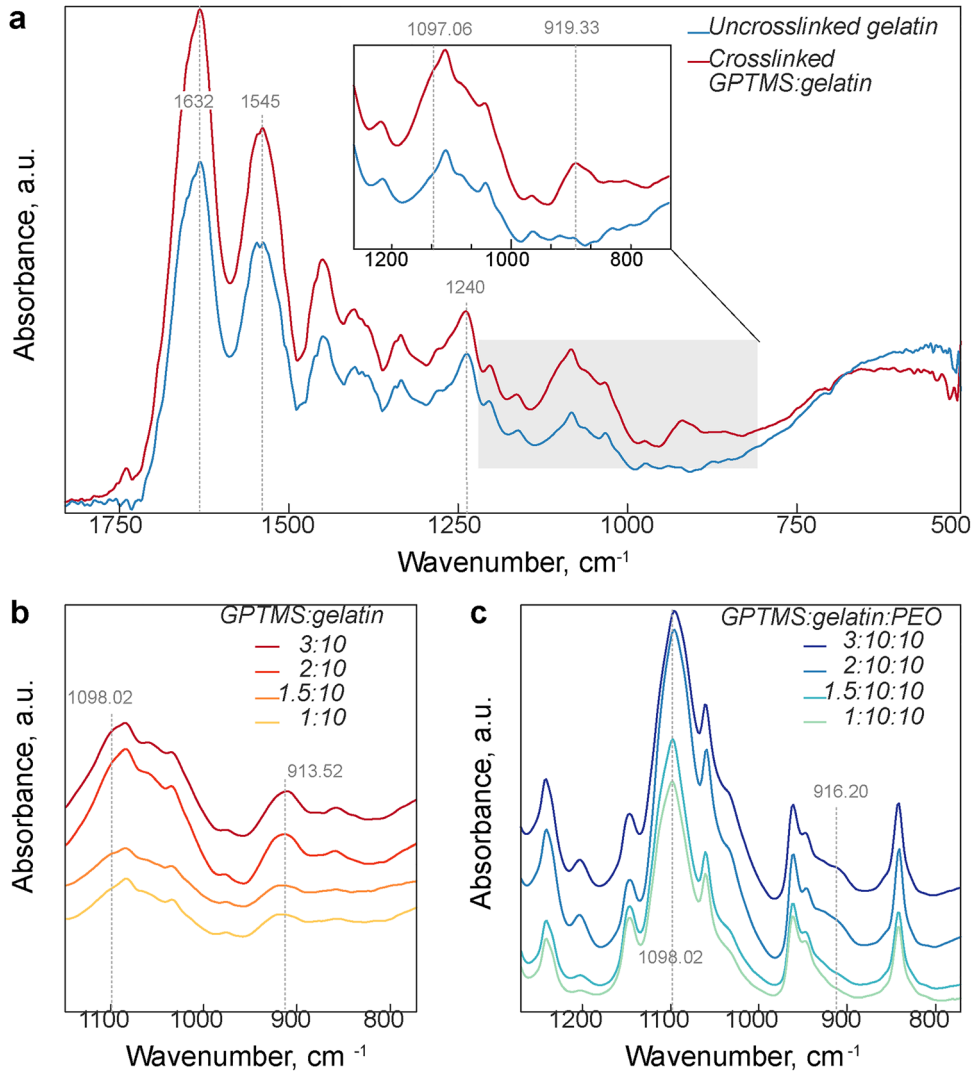

Fig. 3 (a) FTIR spectra of uncrosslinked and GPTMS-crosslinked gelatin. Amide I (C═O stretch) ~1632 cm^{-1}, amide II (N–H bending) ~1545 cm^{-1}, and amide III (C–N stretch) ~1240 cm^{-1} are marked. (b) FTIR spectra of crosslinked gelatin samples with varying GPTMS concentrations. (c) FTIR spectra of crosslinked gelatin samples with varying GPTMS concentrations in the presence of PEO. Crosslinking characteristic bands at ~920 cm^{-1} (Si–OH) and ~1098 cm^{-1} (Si–O–Si) are marked. Overlap of siloxane and PEO C–O–C bands is indicated at ~1100 cm^{-1}.

in the ninhydrin assay, the actual gelatin amount within the samples varied across different sample groups. For instance, GG:PEO1% samples had the highest gelatin content, whereas GG:PEO4% samples contained approximately two-thirds of that amount. As a result, absorbance levels correlated with the gelatin content in the samples reacting with the ninhydrin reagent, rather than reflecting true crosslinking efficiency. Therefore, to account for variations in gelatin content across samples, the free amino group amounts calculated from the absorbance values were normalized according to the weight ratio of gelatin in each film. Similar methods have been reported in studies investigating the effect of plasticizers on crosslinking efficiency in gelatin films, supporting the need for careful sample normalization to ensure accurate crosslinking measurements.[56,59]

Contrary to our initial hypothesis that PEO would not interfere with the crosslinking reaction between the GPTMS epoxy groups and gelatin chains, we observed a gradual increase of crosslinking with higher PEO concentrations. This could indicate the potential hydrogen bonds formed between gelatin amine groups and PEO ether oxygens that consumed a portion of the remaining amine groups, decreasing the number of free gelatin amine groups.

Although the crosslinking extent increased over time in all samples, the effect of drying time was not statistically significant. This increase was more prominent in samples with lower PEO due to higher water content, thus requiring more time until fully condensed.

3.3. Effect of PEO concentration, drying time, and temperature on crosslinking efficiency and chemical composition of GG:PEO films

Chemical characteristics in GG:PEO samples with varying PEO concentrations were assessed by FTIR, maintaining a 2 : 10 w/w

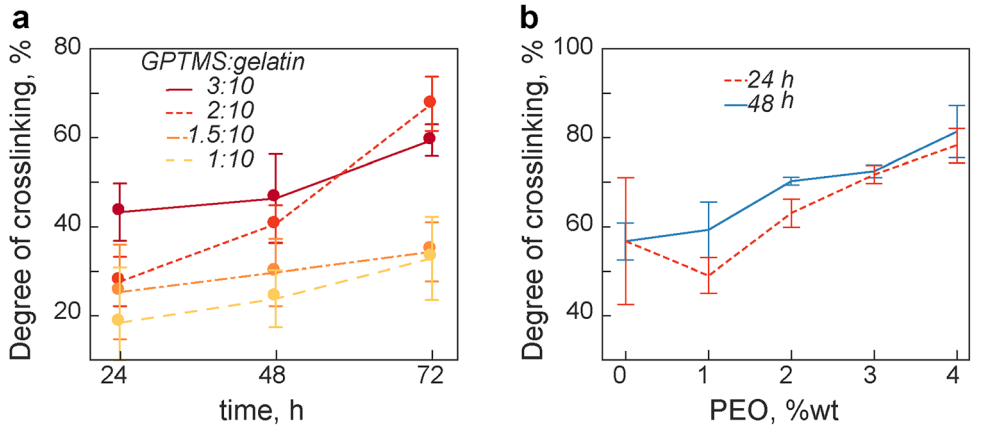

Fig. 4 Degree of gelatin crosslinking in films with different compositions. (a) Crosslinking as a function of different mass ratios of GPTMS to gelatin amino groups over various drying periods. (b) Degree of crosslinking for samples with a fixed 2 : 10 GPTMS mass ratio and varying PEO concentrations (wt%).

ratio of GPTMS to gelatin. Samples with PEO to gelatin mass ratios below 1 ($W_{PEO}/W_{gelatin} < 1$) were specifically evaluated to ensure that gelatin remained dominant during the conjugation with silanol groups and the formation of siloxane bonds. Samples were prepared by air-drying for different periods with some subjected to an additional 30-minute heat treatment. Prolonged heat treatment was avoided as it caused the films to become highly stiff and brittle, especially at lower PEO concentrations.

Fig. 5 shows the effect of temperature and drying period on the chemical composition and crosslinking characteristic bands in crosslinked gelatin films and hybrid films with PEO. As shown, silanol (Si–OH) bond peaks around 920 cm^{-1} band were observed in all the samples, indicating successful hydrolysis of trimethoxy groups (–OCH_3) of GPTMS leading to an abundance of active silanol groups available to conjugate with gelatin amine groups in the presence of PEO. However, with the increasing concentration of PEO, the characteristic bands at 1100 cm^{-1} corresponding to siloxane (Si–O–Si) bands became less prominent. This reduction in intensity was likely due to the overlapping peaks around 1100 cm^{-1} region with PEO characteristic bands. Alternatively, PEO might sterically hinder the interaction between gelatin amine groups and active silanol groups by acting similarly to a plasticizer and decreasing the intermolecular forces and increasing polymer chain mobility, further contributing to the diminished siloxane peak.[60]

When comparing GG:PEO spectra with different drying times, the characteristic siloxane peak around 1100 cm^{-1} in GGPEO0% films had higher intensity with increasing drying time (labelled as 12 h, 24 h, and 48 h in Fig. 5a), suggesting a higher degree of conjugations and crosslinked chains. For GG:PEO1%–4% samples, the FTIR spectra indicated that longer drying times contributed to more prominent silanol characteristic bands, particularly in GG:PEO1% and GG:PEO2% samples, where the lower PEO concentration may have allowed for a greater volume of water molecules to remain in the gels, prolonging the drying phase. At 24 h and 48 h time points,

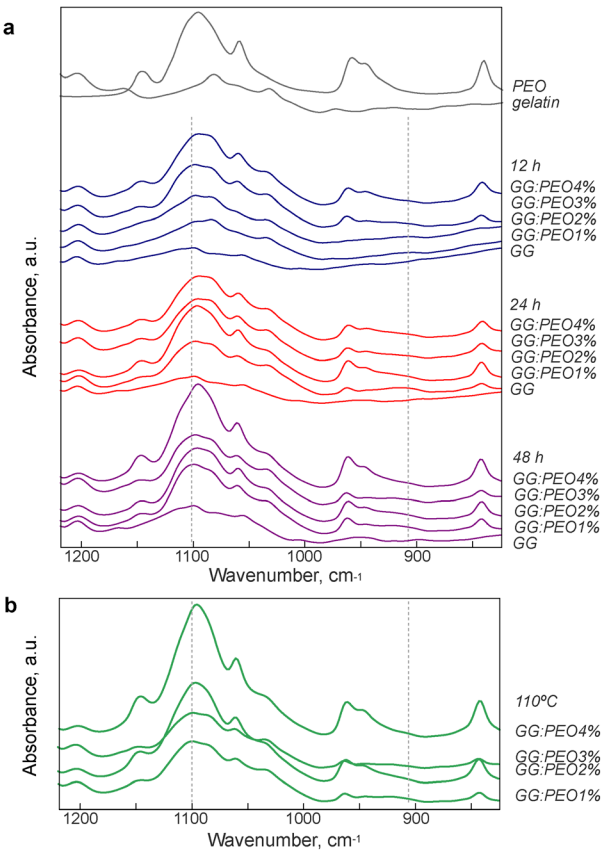

Fig. 5 FTIR spectra for GG:PEO films with varying PEO concentration, drying period and temperature. (a) FTIR spectra for films prepared after air-drying for 12 h (blue), 24 h (red), 48 h (purple) durations. Pure PEO and gelatin (5% w/v) spectra were included for reference. (b) FTIR spectra present samples undergoing heat-treatment at 110 °C for 30 min after 48 h air-drying. Dotted lines at ~920 and ~1100 cm^{-1} indicate characteristic peaks corresponding to Si–OH and Si–O–Si bands, respectively.

the siloxane bands at ~1100 cm^{-1} broadened compared to the 12 h time point. This is likely due to a greater extent of crosslinking achieved by more complete solvent evaporation.

The water content and drying status of the samples were further evaluated (data not shown) by analyzing the intensity ratio between the 3300 cm^{-1} band, associated with O–H stretching and the amide II and amide III peaks at 1545 and 1240 cm^{-1}, respectively. Water molecules contribute to the 3300 cm^{-1} band due to the O–H stretching, forming a broad, intense band resulting from the overlapping of gelatin amide A band and water O–H stretching.[61]

The intensity ratio between the 3300 cm^{-1} peak and gelatin characteristic peaks remained significantly high after 12 h of drying (data not shown), confirming the high water content in samples and incomplete crosslinking.

Heat-treated samples (Fig. 5b) showed no significant difference in crosslinking characteristic bands, suggesting that full crosslinking was achieved after 48 h air-drying, with no further condensation induced by the high temperature treatment.

3.4. Effect of PEO concentration on hydrophilicity, swelling, and dissolvability of crosslinked gelatin films

Swelling and water uptake are important factors in the design and application of biodegradable materials, reflecting fluid absorption, and degradation through hydrolysis.[62] Swelling is also an indirect measure of crosslinking, as the degree of swelling is inversely proportional to the number of crosslinks per unit volume. The degree of swelling was measured in solvent-cast GG:PEO films with varying PEO concentrations. GG:PEO0% films were also tested as a reference. Fig. 6a shows a significant rise in swelling with increasing PEO concentration up to GG:PEO2%. Swelling rates were hindered at higher PEO densities as the films began to dissolve significantly in solution. Samples without PEO showed an average swelling rate of 173.29% ± 10.7%, while this value increased to 641.60% ± 60.36% for GG:PEO2%. Crosslinking is typically associated with lower levels of water uptake as the formation of additional bonds leads to a denser polymer network with reduced free space and limited motility for water molecules.[55,63] Therefore, it can be inferred that PEO polymer chains in GG:PEO films were likely not significantly conjugated to GPTMS or gelatin network, allowing them to maintain their hydrophilic properties and contribute to increased swelling.

Fig. 6b shows the dissolvability levels of GG:PEO films in PBS as a function of PEO concentration in GG:PEO samples. Uncrosslinked gelatin films were completely dissolved in the solution and therefore were not included. GG:PEO4% samples

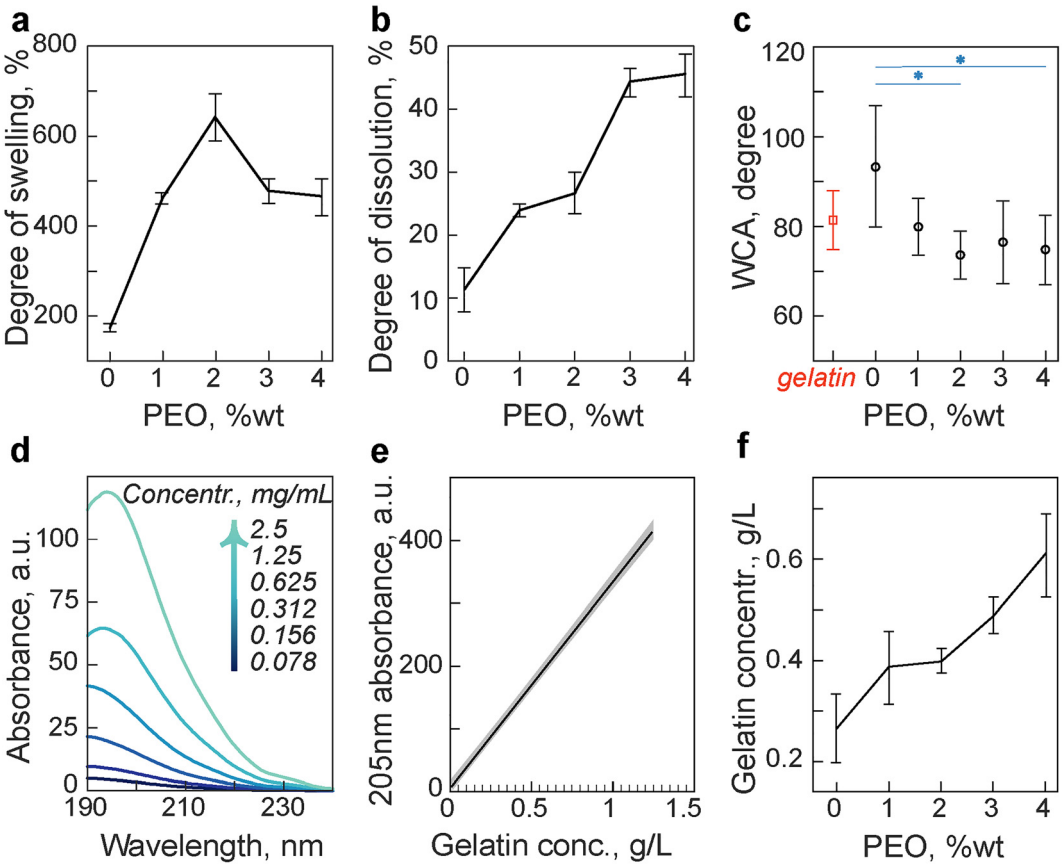

Fig. 6 (a) Degree of swelling and (b) dissolubility for GG:PEO films with varying concentrations of PEO. (c) Water contact angle (WCA) for pure gelatin and GG:PEO films with various concentration of PEO. Statistical significance was considered for $P \leq 0.05$ (*). (d) UV absorption spectra for gelatin with different concentrations. (e) Standard curve for UV absorption at 205 nm as a function of gelatin concentrations. (f) Gelatin leaching rates of GG:PEO films immersed in PBS for 24 h. Gelatin concentrations were calculated using the standard curve in (e). All data points are in triplicates and are presented as average value ± standard deviation.

showed the highest dissolvability, with a rate of 45.66% ± 3.40%. This value decreased to 11.38% ± 3.57% in GG:PEO0% samples, which did not contain any PEO. These values were closely correlated to the total PEO content in each sample, suggesting that the majority of the weight loss was due to PEO dissolution, consistent with the water-soluble nature of the PEO polymer.

Modulating the swelling and dissolution behavior of GG:PEO films is critical for achieving controlled release of antimicrobial agents in wound dressings. While the incorporation of antimicrobials in the polymer network already provides a baseline sustained release, regulating swelling and dissolution allows for additional control over release kinetics. By adjusting the GG:PEO composition, we can fine-tune the hydrogel responsiveness and better align antimicrobial delivery with the severity and extent of infection.

The effect of PEO concentration on the hydrophilic characteristics of GG:PEO films was evaluated through contact angle measurements, a standard method for assessing surface wettability. Surface wettability plays a crucial role in biomaterials, as it significantly impacts their functionalisation, biocompatibility, and interaction within biological environments.[64,65] Additionally, while bacterial attachment depends on multiple factors including surface roughness, charge, and cell type, studies have shown that intermediate wettability (contact angles between 70–90°) generally favors higher bacteria or cell adhesion.[66,67] As demonstrated in Fig. 6c, crosslinking gelatin films increased surface hydrophobicity (81.30° ± 6.64° for gelatin, 93.33° ± 13.58° for GGPEO0%). The incorporation of PEO into the crosslinked gelatin matrix enhanced hydrophilicity, with a more pronounced effect in GG:PEO2% and GG:PEO4% films, which presented significantly higher wettability compared to gelatin films.

Despite the inherent hydrophilicity of gelatin molecules, during the film formation, the hydrophobic sites tend to move towards the solid–air interface, promoting surface hydrophobicity.[68] Moreover, GPTMS reduces wettability by introducing hydrophobic siloxane chains.[69] On the other hand, ether groups (–O–) in PEO readily attract water molecules and contribute to the enhanced wettability in GG:PEO films due to the increased availability of hydrophilic sites on the polymeric surface, supporting better interaction with aqueous environments and regulating antimicrobial release kinetics.

3.5. Gelatin leaching and release

The degree of gelatin leaching was investigated through UV spectrophotometry to provide insights into the stability and integrity of the GG:PEO films and the impact of PEO on gelatin release. In the previous section it was shown that increased PEO content led to higher dissolution rates. Nevertheless, it was not clear whether PEO dissolution also induced gelatin leaching. The near-UV absorption spectrum is typically used to measure the concentration of aromatic amino acids, primarily tyrosine and tryptophan, in protein samples.[70,71] However, aromatic side chains in gelatin are not predominant and do not provide a characteristic near-UV absorbance spectrum.

The most frequent chromophore in any proteins, including gelatin, is the amide group in the peptide backbone. This group contains two major electronic transitions: a strong $\pi \rightarrow \pi^*$ transition of the amide bonds with maximum absorbance at 195 nm, and a second weaker $n \rightarrow \pi^*$ transition of a non-bonding (n) electron near ~220 nm.[72,73] These absorbance peaks in the far-UV region were also observed in the present work, showing a bell-shaped spectrum with a major peak between 190–220 nm and a smaller peak in the 220–230 nm range (Fig. 6d). The primary absorption peak slightly red shifted with increasing gelatin concentrations, which could be attributed to intermolecular interactions, aggregation and conformational changes, or pH effects.[70,74,75] A similar shift in the far-UV spectrum of collagen with increasing concentration was reported by Na *et al.*[76] Meanwhile, PEO did not display any major absorption peaks in the UV region, posing no interference when measuring gelatin concentrations in GG:PEO samples (data not shown).

Since the slight red-shifts were observed in the primary absorption peak, we evaluated the absorbance values across 190–240 nm wavelength range for their linear correlation with gelatin concentration, and 205 nm was selected as the optimal wavelength for constructing the standard curve and for subsequent quantification of gelatin leaching. Fig. 6e shows this linear relationship between absorbance at 205 nm and gelatin concentration with a calculated correlation coefficient R = 0.9966.

Consistent with the increased dissolvability rates observed at higher PEO concentrations, we also observed a corresponding increase in the gelatin leaching rate as PEO content increased (Fig. 6f). This phenomenon can likely be attributed to the enhanced water absorption capacity of PEO molecules, which resulted in greater interaction between gelatin and water, thus accelerating gelatin leaching into the solution. The hydrophilic nature of PEO allows it to absorb significant amounts of water, swelling within the film and creating pathways that enable gelatin molecules to diffuse out more readily. However, when the amount of leached gelatin was correlated to the total gelatin content in the films (250 mg), the absolute values remained relatively low. This suggests that, despite the increased leaching with higher PEO concentrations, the overall loss of gelatin from the films was minimal. The effective crosslinking of gelatin by GPTMS resulting in the formation of siloxane bonds, appears to effectively control the hydrolysis and dissolution of gelatin in aqueous media, thereby preserving the structural integrity of the films despite the presence of PEO.

3.6. Mechanical studies

Mechanical testing is essential for evaluating the structural integrity and performance of biomaterials such as wound dressings. These tests assess how materials respond to forces by assessing their strength, flexibility, and ability to stretch. These properties are essential to ensure that materials can withstand handling, conform to biological structures, and maintain their functionality over time.

The mechanical properties of GG:PEO films were investigated as a function of the gelatin/PEO ratio. Uncrosslinked pure gelatin films were also tested for comparison. Representative stress–strain curves are shown in Fig. 7a. Young's modulus, tensile strength, and strain at break were derived from the stress–strain curves (Fig. 7b and c). As shown, the highest tensile strength was in samples without PEO (44.19 ± 10.78 MPa for gelatin, 42.93 ± 12.26 MPa for GG:PEO0% film), while it tended to decrease as the PEO content increased, indicating that PEO softened the film matrix. Higher PEO content likely reduced intermolecular forces between protein chains, making it more flexible at the expense of strength.

Similar to tensile strength, Young's modulus values decreased by increasing PEO concentration. GG:PEO0% film had a slightly higher moduli compared to gelatin films, which is due to the formation of shorter and stronger bonds. However, this increase was not statistically significant ($P > 0.05$). While gelatin and GG:PEO0% films exhibited very high stiffness, the modulus was decreased more than two-fold in samples with higher PEO content. This reduction in Young's modulus can be attributed to the increased spacing and free volume induced by the addition of PEO in a dense crosslinked gelatin network.

It is worth noting that, both tensile strength and Young's modulus reached a minimum at GG:PEO3% before stabilizing. The values were slightly higher for GG:PEO4% but it was not significant ($P > 0.05$).

Strain at break values represent elongation before the sample permanently breaks. Materials with higher elongation rates are less brittle and more ductile, as the films can withstand more deformation without fracturing. Fig. 7c shows the strain at break values for GG:PEO films. With increasing PEO concentration until 2%, the strain at break followed an increasing trend. Crosslinked gelatin films have a rigid structure due to the high number of intramolecular bond forces due to crosslinking. Introducing a low amount of PEO likely increases free volume as PEO molecules situate themselves around the gelatin chains, inducing flexibility and ductility as a plasticizer. Although PEO is not conventionally cited as a plasticizer in gelatin systems, the observed reduction in tensile strength and stiffness, alongside increased elongation at break at moderate PEO concentrations, suggest plasticizer-like effects. However, the crystallinity of high-M_w PEO and lack of thermal characterisation (*e.g.*, T_g analysis) prevent definitive confirmation of plasticizing action.

A less expected behavior was observed for samples with higher PEO content (GG:PEO3% and GG:PEO4%). Unlike GG:PEO1% and GG:PEO2%, higher PEO addition did not improve the ductility of GG:PEO0% films but made them more brittle. This transition could be explained by lack of miscibility

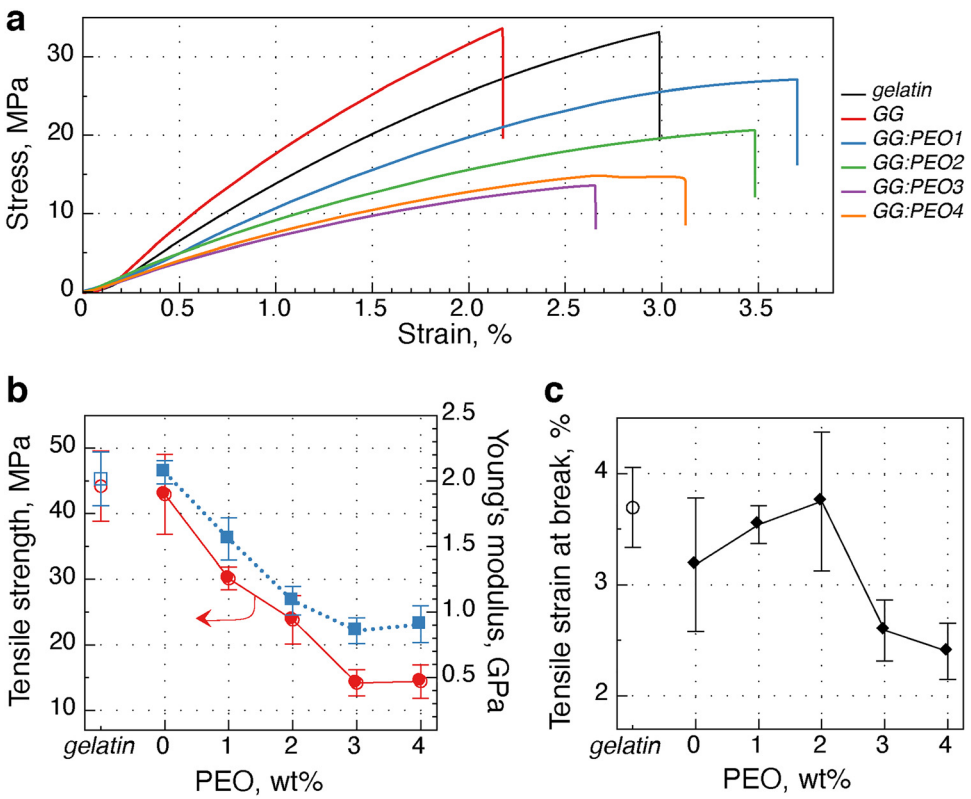

Fig. 7 Mechanical test for GG:PEO films. (a) Representative stress–strain curves for gelatin, GG, GG:PEO1%–4% films. (b) Tensile strength (red) and Young's modulus (blue) graphs as a function of PEO concentration obtained from stress–strain curves. (c) Strain at break graph as a function of PEO concentration obtained from stress–strain curves. Pure gelatin films were tested for comparison. All values in (b) and (c) are expressed as average value ± standard deviation.

of PEO and gelatin. As a result, blends with similar gelatin and PEO contents have heterogeneous morphology that induce early fracture and lower ductility. Similar results were reported for chitosan and PEO blends in the literature.[77,78] Another possible explanation for the poor elongation of GG:PEO3% and GG:PEO4% films could be the crystallinity of PEO. PEO is a semicrystalline polymer, and while gelatin chains might impede the crystallization through hydrogen bonding between ether and amino groups, crystallization may still occur with higher PEO content.[79]

Toughness of the films were also investigated as a complementary mechanical metric. The mean toughness values for gelatin, GG, and GG:PEO1–4% films were 430.6 ± 162.9, 372.5 ± 254.4, 290.1 ± 43.7, 281.2 ± 22.0, 104.4 ± 66.7, and 125.2 ± 51.0 J m^{-3}, respectively. Toughness did not correlate linearly with tensile strength or strain at break, as it depends on the combined contribution of both parameters. Although overall toughness decreased with increasing PEO content up to 3%, a slight increase was observed for the GG:PEO4% samples. This behaviour is attributed to necking seen in some GG:PEO4% specimens, where stress gradually declined after the onset of localized yielding rather than showing abrupt brittle fracture, therefore increasing the area under the curve and the apparent toughness.

For an ideal wound dressing material, the film must have good tensile strength and high elongation at break.[80] Our results indicated that GG:PEO2% films exhibit improved ductility and reduced stiffness and tensile strength compared to GG:PEO0% films. Moreover, as observed visually, unlike GG:PEO0% films, GG:PEO films did not fracture upon bending, providing ease of application as potential wound dressings. Although the tensile at break values were low in general, this was attributed to the dimensions of our samples, which had a length-to-width ratio of 1.4, thus limiting the stretchability of the specimen during the test.

3.7. Characterisation and antimicrobial activity of MMC integrated GG:PEO films

3.7.1. Film morphology and elemental analysis. GG:PEO biopolymer films showed adjustable physicochemical and mechanical properties, making them useful for antimicrobial applications. Their swelling, degradation, and structural behavior can be tailored to control the release of active agents and improve interaction with bacterial biofilms.[8,81] However, the polymers themselves do not have antimicrobial properties and do not interfere with bacterial growth (Fig. 9b). Therefore, we employed a novel multifunctional metal complex (MMC) in GG:PEO films that present antibacterial activities against the wound opportunistic pathogen *P. aeruginosa* due to its silver and copper compounds.

Scanning electron microscopy (SEM) and energy-dispersive X-ray spectroscopy (EDS) were conducted to confirm the morphological consistency and chemical composition of the films containing 2% w/w of the MMC. EDS mapping was used to qualitatively verify the presence and approximate surface distribution of MMC-based metal signals across formulations.

SEM images in Fig. 8 revealed distinct morphological differences across the series of GG:PEO films. With increasing PEO content, the surface topography became more porous and disordered, reflecting the shift from a dense, crosslinked gelatin matrix to a more phase-separated structure. Films with higher gelatin content appeared smoother and more uniform, while those with higher PEO ratios showed visible phase separation and heterogeneity, indicative of the immiscible behavior between gelatin and PEO. These images were consistent with prior observations in MMC-free samples and confirmed that MMC incorporation did not have any significant effect on the film-forming process.

As shown in Table 2, EDS elemental mapping provided further insight into film composition. As expected, the elemental spectra were dominated by carbon (C) and oxygen (O), derived from the organic backbone of both gelatin and PEO. Their uniform distribution across all samples suggests good mixing and homogeneity at the macro scale. The silicon (Si), resulting from gelatin crosslinking by GPTMS, gradually decreased with increasing PEO content, confirming the reduction in crosslinked gelatin as the PEO proportion increased.

Importantly, silver (Ag) elemental maps confirmed the successful and uniform incorporation of MMC into all film variants. Despite differences in morphology and composition, silver content remained consistent across samples, indicating that the MMC concentration was reliably maintained at 2% w/w. This eliminates the possibility that any variation in antimicrobial activity is due to uneven MMC loading but rather due to the physical and structural properties and release behaviors.

Together, the SEM and EDS results confirmed that the MMC-loaded films were structurally and chemically consistent, with compositional trends that reflect the intended gelatin/PEO ratios. These findings established the basis for interpreting the subsequent antimicrobial studies.

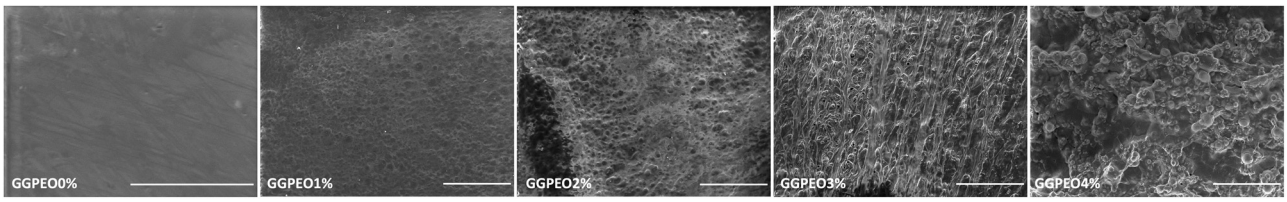

Fig. 8 SEM micrographs for GG:PEO films loaded with 2% w/w MMC. Figures from left to right represent GG:PEO0%–4% samples, respectively. Scale bars indicate 500 μm.

Table 2 EDS elemental map analysis for GG:PEO films loaded with 2%w/w MMC. Values (%wt) represent the relative abundance of elements in the films

Sample	Carbon (C)	Oxygen (O)	Silicon (Si)	Silver (Ag)
GGPEO0%	75.0% ± 4.0%	14.8% ± 1.1%	6.6% ± 0.4%	1.7% ± 0.5%
GGPEO1%	76.4% ± 1.1%	16.2% ± 1.0%	5.4% ± 0.3%	2.0% ± 0.7%
GGPEO2%	74.3% ± 4.1%	15.9% ± 1.2%	4.5% ± 0.3%	2.6% ± 0.5%
GGPEO3%	74.9% ± 0.9%	19.3% ± 0.8%	3.9% ± 0.2%	2.0% ± 0.5%
GGPEO4%	74.0% ± 1.0%	19.7% ± 0.9%	3.6% ± 0.2%	2.0% ± 0.5%

3.7.2. Kirby-Bauer disc diffusion test. MMC loaded GG:PEO films with the same size and thickness were tested against *P. aeruginosa* PA14, one of the most prevalent wound-related pathogens, using the standard disc diffusion method. GG:PEO films without MMC were used as positive control. It was shown that all the MMC loaded GG:PEO films had some degree of inhibition zone, confirming that the MMC is indeed released from the films and is active against this Gram-negative strain. On the other hand, GG:PEO films with no MMC did not show any antimicrobial activities (Fig. 9a and b). When comparing the inhibition zone diameters among different GG:PEO films against *P. aeruginosa*, an increasing trend with increasing PEO/gelatin ratio in film composition was observed. Compared to GG:PEO0% films, the inhibition zone against *P. aeruginosa* was significantly larger when exposed to GG:PEO3% and GG:PEO4% films ($p < 0.05$). The maximum zone of inhibition against *P. aeruginosa* was observed in GG:PEO4% films with a diameter of 18.10 ± 0.54 mm.

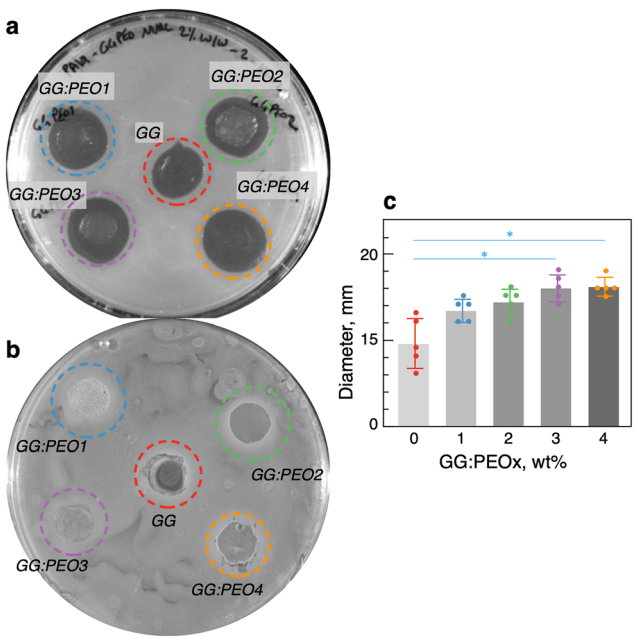

Fig. 9 Disc diffusion test for MMC loaded GG:PEO films. Representative images of agar plates with *P. aeruginosa* exposed to GGPEO(0–4%) films with (a) 2% w/w MMC and (b) agar plates exposed to GGPEO(0–4%) films without MMC are presented as positive control. (c) Diameters of zones of inhibitions for *P. aeruginosa* plates exposed to 2% w/w MMC loaded GG:PEO films. Statistical significance was considered for $P \leq 0.05$ (*). $N = 5$, data presented as average value ± standard deviation.

In addition to *P. aeruginosa*, disk diffusion tests were also performed against *Staphylococcus aureus* (MRSA). The MMC-loaded films showed distinct inhibition zones against MRSA as well, confirming the efficacy of the released metal complex against both Gram-negative and Gram-positive bacteria that could be tuned by gelatin-to-PEO ratio (Fig. S1).

Overall, higher PEO/gelatin content ratio showed greater inhibition zones, which can be attributed to higher swelling and faster diffusion of the antimicrobial agent. This suggested that MMC release was primarily governed by water absorption and swelling-induced diffusion from the GG:PEO films. However, a contribution from initial surface-bound MMC or contact-based inhibition cannot be completely excluded. None of the zones appear excessively large or purely contact-based but rather demonstrated discrete and noticeable clearing. This suggested some degree of sustained release from the discs rather than a single immediate pulse of MMC.

3.7.3. Growth curves and resazurin viability test. Disc diffusion test provided valuable insights into MMC loaded film interactions with the bacteria and how film composition controlled the inhibition rates, as increasing PEO/gelatin ratio in film structure demonstrated improved MMC effectiveness against *P. aeruginosa* after 24 h incubation. However, the release kinetics were not yet fully understood. We used a resazurin viability assay to further investigate viability of bacterial cells exposed to GG:PEO films with and without MMC over time. Viable bacteria, which are metabolically active, reduce resazurin, a weakly fluorescent blue-purple compound to resorufin, a pink molecule that is highly fluorescent. In contrast, non-viable bacteria cannot catalyse this reduction, and consequently no colour shift or increase in fluorescence intensity is observed.

Additionally, a pre-screening experiment was conducted to identify the effective MMC concentration range against *P. aeruginosa*. Growth curves were measured by monitoring OD600 over 24 h using GG:PEO0% films loaded with varying MMC concentrations (from 30 to 3000 ppm MMC), starting from a lower initial bacterial density corresponding to approx. 10^6 CFU per ml. As shown in Fig. 10a, MMC concentrations ≥1000 ppm completely inhibited *P. aeruginosa* growth, while 100–300 ppm resulted in a delayed exponential phase, leading to a decrease in bacterial density but not inactivating all of the bacteria cells. Area under the curve values also confirmed the inhibitory effect of MMC release on bacterial growth with increasing antimicrobial concentration. These helped with the MMC dose selection for subsequent resazurin assays, which were conducted at a higher initial inoculum to monitor metabolic viability in more established bacterial populations.

After determining the effective antimicrobial concentrations, the effect of film composition and the PEO/gelatin ratio on MMC release profiles was investigated by measuring bacterial viability. MMC in three different concentrations (MMC100, MMC300, and MMC1000) was incorporated into GG:PEO0%, GG:PEO2%, and GG:PEO4% films and bacteria viability was screened for 24 h using the resazurin assay. For comparison, films with no MMC were also treated with bacteria. After 24 h

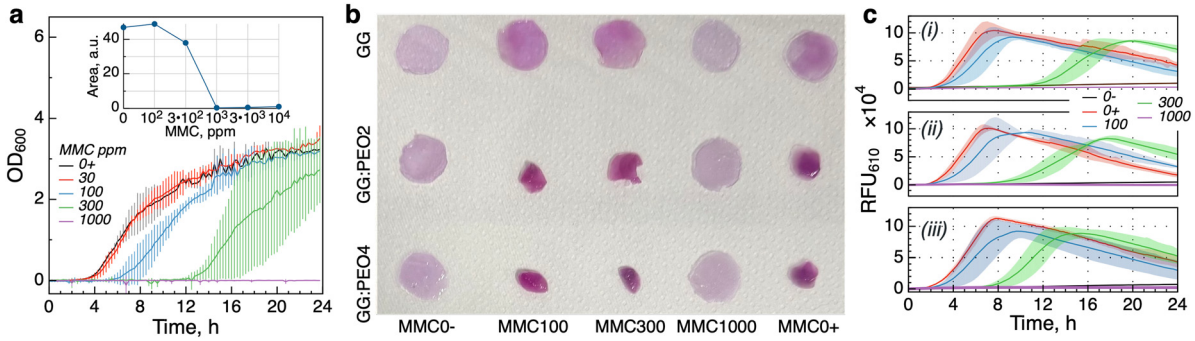

Fig. 10 Antimicrobial activity kinetics in MMC loaded GG:PEO films in the presence of *P. aeruginosa*. (a) Growth curves and area under the curve for *P. aeruginosa* when exposed to GGPEO0% films with varying MMC concentrations. (b) GGPEO0%–2%–4% films with varying MMC concentrations after being treated with *P. aeruginosa* in the presence of resazurin for 24 h. (c) Antibacterial effect of (i) GG:PEO0%, (ii) GG:PEO2%, and (iii) GG:PEO4% with 0 ppm (red), 100 ppm (blue), 300 ppm (green), and 1000 ppm (purple) loaded MMC against *P. aeruginosa* viability over 24 h. Negative controls (0−) with no bacteria were tested for comparison (black). All the data were repeated three times (biological replicates) and are presented as average value ± standard deviation.

measurement, samples were removed from the solutions to investigate the effect of bacterial culture on GG:PEO films. As shown in Fig. 10b, the apparent colour difference confirmed the metabolic reduction with the zero or intermediate MMC samples. Samples in blank nutrient media maintained their structural integrity and did not have any visible deformation. Similarly, GG:PEO0% films remained in their original form regardless of the presence of MMC. GGPEO2% and GG:PEO4% films, were subject to disintegration as a significant portion was dissolved in the bacterial culture. It was shown in previous sections that film dissolution significantly increased with increasing PEO/gelatin content. However, when comparing with the negative control sample, additional dissolution was observed due to gelatin consumption by *P. aeruginosa* through enzyme degradation.[82]

As shown in Fig. 10c, for the films with no MMC, bacterial viability increased over time and reached a maximum level, corresponding to high metabolic activity and population growth. The subsequent steady drop could be attributed to a further reduction to a non-fluorescent compound (dihydroresorufin), resazurin co-depletion, or accumulation of bacterial by-products. Samples with intermediate MMC concentration maintained similar trend in metabolic profiles but resulted in significant delays and reduced bacterial viability (max value). While the max viability occurred at approx. 8 h (468 min) with 112 784 ± 3716.0 RFU for GG:PEO4% films with no MMC, this value was 92 437.17 ± 11 662.72 for MMC100 at approx. 10 h (588 min), and 88 898 ± 8060.1 for MMC300 at approx. 15 h (914 min). A similar trend also occurred with GGPEO0% and GGPEO2% films. Table 3 depicts the percentage of max viability and its time with respect to GG:PEO0%–2%–4% films with no MMC. When combining the effect of intensity attenuation due to lower viability with delay in bacterial growth and metabolic activity GG:PEO4% films with MMC100 showed the highest antimicrobial activity based on the area under curve (AUC) values among the films. For MMC300 concentration, GG:PEO0% had the lowest AUC percentage among the films. MMC1000 values were close to zero among all the films.

When comparing the films, film composition did not significantly affect the viability when exposed to MMC100 samples. However, GG:PEO0% films with MMC300 led to a longer delay in viability expansion compared to GG:PEO2% and GG:PEO4% samples. MMC1000 samples completely inactivated metabolic activity in all the films, showing flat viability curves for 24 h.

Overall, the onset and intensity of the metabolic activity signal were closely tied to the antimicrobial release kinetics of the films. Although all MMC300 loaded GG:PEO films contained the same moderate concentration of MMC (not high enough to fully inhibit growth), differences in film composition influenced how quickly bacteria recovered and resumed activity. Films with higher PEO content, which swell and dissolve more rapidly, likely released MMC more quickly but also exhausted it sooner, allowing bacterial growth to resume earlier. This resulted in a faster appearance of the resazurin signal

Table 3 Comparison between viability percentage, peak delay, and area under curve (AUC) percentage for GG:PEO0%–2%–4% with MMC100-1000 based on resazurin fluorescence measurements. Percentage values were calculated with respect to the values for samples with no MMC. Peak delays were calculated by subtracting the peak times for samples with no MMC as reference. NA indicates no peak selection in curves where no growth was observed

	GGPEO0%			GGPEO2%			GGPEO4%		
	MMC100	MMC300	MMC1000	MMC100	MMC300	MMC1000	MMC100	MMC300	MMC1000
Peak RFU, %	88.92	82.17	3.02	92.60	81.97	1.05	81.96	78.84	2.18
Peak RFU delay, min	90	716	NA	201	637	NA	120	431	NA
AUC, %	81.47 ± 0.26	51.36 ± 0.18	3.44 ± 0.06	104.78 ± 0.35	67.29 ± 0.20	0.75 ± 0.023	78.34 ± 0.31	65.30 ± 0.21	3.01 ± 0.01

in high PEO content films. In contrast, GGPEO0% films exhibited slower, more sustained release due to gelatin hydrolysis, delaying bacterial recovery and leading to a later onset of the resazurin signal. These differences in signal timing reflect how the film matrix modulates antimicrobial exposure in earlier time points and ultimately affects the dynamics of bacterial suppression.

Together, disc diffusion and viability test results indicate that while PEO enhances early antimicrobial diffusion by faster swelling and dissolution, gelatin contributes to sustained release and longer lasting inhibition.

To relate antimicrobial performance to metal-ion availability, a silver-release assay was performed for MMC-loaded GG:PEO2% films (1% w/w MMC). The films displayed a biphasic release profile with an initial burst within the first 15 min followed by a slower diffusion-controlled phase over 24 h (Fig. S2 and Table S1). The cumulative silver flux averaged approximately 23.5 μg cm^{-2} day^{-1}, which falls within the range commonly reported for active silver dressings.[83] This indicates that the MMC-loaded films are capable of releasing clinically relevant silver levels while maintaining sustained antimicrobial activity. Given that this preliminary study was limited to one representative formulation, extended compositional studies will be undertaken in future work.

4. Conclusions

The effective management of chronic wound infections remains a significant clinical challenge, particularly with rising antimicrobial resistance. This study successfully demonstrates the design and characterisation of crosslinked gelatin–polyethylene oxide hybrid films (GG:PEO), as a robust tunable platform for responsive antimicrobial delivery. With precise modulating of the gelatin/PEO ratio, these biopolymer structures offer tunable mechanical properties, controlled swelling, and dissolution behaviors essential for tailored antimicrobial kinetics.

Incorporating a multifunctional metal complex (MMC) demonstrated significant antimicrobial efficiency against *P. aeruginosa*. The release of MMC from the hybrid matrix can be finely controlled, thus providing larger growth inhibition using higher PEO content and more sustained release of low MMC concentration within the crosslinked gelatin matrix.

Thus, these hybrid films address a critical gap in current biomaterial strategies by combining structural integrity, biocompatibility, and responsive antimicrobial functionality. These complementary findings highlight the potential of GG:PEO films to provide release profiles tailored to different wound environments and broader clinical applications. The versatility and effectiveness of these materials also highlight their potential to reduce the burden of infections thus improving clinical outcomes. Future work will evaluate the cytocompatibility of the MMC-loaded films with skin-relevant cell lines to define safe concentration ranges and confirm their suitability for wound dressing applications.

Author contributions

SS: conceptualization, methodology, investigation, data curation, formal analysis, visualisation, writing – original draft. MS: conceptualization, methodology, resources, supervision, writing – review & editing. RC: methodology, validation, resources, writing – review & editing. JC: conceptualization, supervision, writing – review & editing. MU: conceptualization, supervision, resources, writing – review & editing. SP: supervision, resources, funding acquisition, writing – review & editing. DI: supervision, project administration, funding acquisition, conceptualization, methodology, visualisation, writing – review and editing, corresponding author.

Conflicts of interest

MJS, RC and SLP are employed by 5D Health Protection Group Ltd which holds the IP for the MMC complex used in this study.

Data availability

The data supporting this article have been included as part of the supplementary information (SI). Supplementary information is available. See DOI: https://doi.org/10.1039/d5tb02157j.

All data supporting the findings of this study are available within the article. Raw data are available from the corresponding author upon request.

Acknowledgements

SS was funded by an industry-linked iCASE studentship on the MRC funded Doctoral Training Partnership (DTP) in Interdisciplinary Biomedical Research (MR/R015910/1). The authors would also like to thank Dr Andrea Dsouza (Warwick Medical School) for providing the resazurin dye and offering technical guidance and fruitful discussions regarding resazurin assay. Figures were created and edited using Graphics and Biorender software.

References

1 M. E. Olson, H. Ceri, D. W. Morck, A. G. Buret and R. R. Read, Biofilm bacteria: formation and comparative susceptibility to antibiotics, *Can. J. Vet. Res.*, 2002, **66**(2), 86–92. Accessed May 19, 2025. https://www.ncbi.nlm.nih.gov/pmc/articles/PMC226988/.

2 R. Mirghani, T. Saba and H. Khaliq, *et al.*, Biofilms: Formation, drug resistance and alternatives to conventional approaches, *AIMS Microbiol.*, 2022, **8**(3), 239–277, DOI: 10.3934/microbiol.2022019.

3 E. Naseri and A. Ahmadi, A review on wound dressings: Antimicrobial agents, biomaterials, fabrication techniques, and stimuli-responsive drug release, *Eur. Polym. J.*, 2022, **173**, 111293, DOI: 10.1016/j.eurpolymj.2022.111293.

4 Y. Xiong, Y. Xu and F. Zhou, *et al.*, Bio-functional hydrogel with antibacterial and anti-inflammatory dual properties to

combat with burn wound infection, *Bioeng. Transl. Med.*, 2023, **8**(1), e10373, DOI: 10.1002/btm2.10373.
5 Y. C. Lin, C. Y. Lee and J. R. Jones, *et al.*, Sustained Antibiotic Release from Biodegradable Gelatin–Silica Hybrid for Orthopedic Infections, *Adv. Funct. Mater.*, 2024, **34**(49), 2409491, DOI: 10.1002/adfm.202409491.
6 S. Mohanto, S. Narayana and K. P. Merai, *et al.*, Advancements in gelatin-based hydrogel systems for biomedical applications: A state-of-the-art review, *Int. J. Biol. Macromol.*, 2023, **253**(Pt 5), 127143, DOI: 10.1016/j.ijbiomac.2023.127143.
7 R. Yasmin, M. Shah, S. A. Khan and R. Ali, Gelatin nanoparticles: a potential candidate for medical applications, *Nanotechnol. Rev.*, 2017, **6**(2), 191–207, DOI: 10.1515/ntrev-2016-0009.
8 S. P. Ndlovu, K. Ngece, S. Alven and B. A. Aderibigbe, Gelatin-Based Hybrid Scaffolds: Promising Wound Dressings, *Polymers*, 2021, **13**(17), 2959, DOI: 10.3390/polym13172959.
9 H. R. El-Seedi, N. S. Said and N. Yosri, *et al.*, Gelatin nanofibers: Recent insights in synthesis, bio-medical applications and limitations, *Heliyon*, 2023, **9**(5), 16228, DOI: 10.1016/j.heliyon.2023.e16228.
10 I. Lukin, I. Erezuma and L. Maeso, *et al.*, Progress in Gelatin as Biomaterial for Tissue Engineering, *Pharmaceutics*, 2022, **14**(6), 1177, DOI: 10.3390/pharmaceutics14061177.
11 T. Billiet, E. Gevaert, T. De Schryver, M. Cornelissen and P. Dubruel, The 3D printing of gelatin methacrylamide cell-laden tissue-engineered constructs with high cell viability, *Biomaterials*, 2014, **35**(1), 49–62, DOI: 10.1016/j.biomaterials.2013.09.078.
12 S. Mohammadzadehmoghadam and Y. Dong, Fabrication and Characterization of Electrospun Silk Fibroin/Gelatin Scaffolds Crosslinked With Glutaraldehyde Vapor, *Front. Mater.*, 2019, **6**, 91, DOI: 10.3389/fmats.2019.00091.
13 C. H. Yao, B. S. Liu, C. J. Chang, S. H. Hsu and Y. S. Chen, Preparation of networks of gelatin and genipin as degradable biomaterials, *Mater. Chem. Phys.*, 2004, **83**(2–3), 204–208, DOI: 10.1016/j.matchemphys.2003.08.027.
14 W. H. Chang, Y. Chang, P. H. Lai and H. W. Sung, A genipin-crosslinked gelatin membrane as wound-dressing material: in vitro and in vivo studies, *J. Biomater. Sci., Polym. Ed.*, 2003, **14**(5), 481–495, DOI: 10.1163/156856203766652084.
15 H. Goodarzi, K. Jadidi, S. Pourmotabed, E. Sharifi and H. Aghamollaei, Preparation and in vitro characterization of cross-linked collagen-gelatin hydrogel using EDC/NHS for corneal tissue engineering applications, *Int. J. Biol. Macromol.*, 2019, **126**, 620–632, DOI: 10.1016/j.ijbiomac.2018.12.125.
16 I. Prasertsung, S. Damrongsakkul and N. Saito, Crosslinking of a Gelatin Solutions Induced by Pulsed Electrical Discharges in Solutions, *Plasma Processes Polym.*, 2013, **10**(9), 792–797, DOI: 10.1002/ppap.201200148.
17 K. Yue, G. Trujillo-de Santiago, M. M. Alvarez, A. Tamayol, N. Annabi and A. Khademhosseini, Synthesis, properties, and biomedical applications of gelatin methacryloyl (GelMA) hydrogels, *Biomaterials*, 2015, **73**, 254–271, DOI: 10.1016/j.biomaterials.2015.08.045.
18 A. Bigi, G. Cojazzi, S. Panzavolta, K. Rubini and N. Roveri, Mechanical and thermal properties of gelatin films at different degrees of glutaraldehyde crosslinking, *Biomaterials*, 2001, **22**(8), 763–768, DOI: 10.1016/S0142-9612(00)00236-2.
19 Y. C. Chen, R. Z. Lin and H. Qi, *et al.*, Functional Human Vascular Network Generated in Photocrosslinkable Gelatin Methacrylate Hydrogels, *Adv. Funct. Mater.*, 2012, **22**(10), 2027–2039, DOI: 10.1002/adfm.201101662.
20 J. Ratanavaraporn, R. Rangkupan, H. Jeeratawatchai, S. Kanokpanont and S. Damrongsakkul, Influences of physical and chemical crosslinking techniques on electrospun type A and B gelatin fiber mats, *Int. J. Biol. Macromol.*, 2010, **47**(4), 431–438, DOI: 10.1016/j.ijbiomac.2010.06.008.
21 O. Mahony, S. Yue and C. Turdean-Ionescu, *et al.*, Silica–gelatin hybrids for tissue regeneration: inter-relationships between the process variables, *J. Sol-Gel Sci. Technol.*, 2014, **69**(2), 288–298, DOI: 10.1007/s10971-013-3214-3.
22 C. Tonda-Turo, E. Cipriani and S. Gnavi, *et al.*, Crosslinked gelatin nanofibres: Preparation, characterisation and *in vitro* studies using glial-like cells, *Mater. Sci. Eng., C*, 2013, **33**(5), 2723–2735, DOI: 10.1016/j.msec.2013.02.039.
23 K. Ulubayram, E. Aksu, S. I. D. Gurhan, K. Serbetci and N. Hasirci, Cytotoxicity evaluation of gelatin sponges prepared with different cross-linking agents, *J. Biomater. Sci., Polym. Ed.*, 2002, **13**(11), 1203–1219, DOI: 10.1163/156856202320892966.
24 R. Rodriguez-Gonzalez, E. Bosch-Rué, L. Díez-Tercero, L. M. Delgado and R. A. Perez, Tailorable low temperature silica-gelatin biomaterials for drug delivery, *Ceram. Int.*, 2022, **48**(19), 28659–28668. Accessed September 3, 2024. https://www.sciencedirect.com/science/article/pii/S0272884222021836.
25 M. Teodorescu, M. Bercea and S. Morariu, Biomaterials of Poly(vinyl alcohol) and Natural Polymers, *Polym. Rev.*, 2018, **58**(2), 247–287, DOI: 10.1080/15583724.2017.1403928.
26 F. M. Vanin, P. J. Sobral, A. do, F. C. Menegalli, R. A. Carvalho and A. Habitante, Effects of plasticizers and their concentrations on thermal and functional properties of gelatin-based films, *Food Hydrocolloids*, 2005, **19**(5), 899–907. Accessed September 3, 2024. https://www.sciencedirect.com/science/article/pii/S0268005X05000044.
27 L. Ma, L. Deng and J. Chen, Applications of poly(ethylene oxide) in controlled release tablet systems: a review, *Drug Dev. Ind. Pharm.*, 2014, **40**(7), 845–851, DOI: 10.3109/03639045.2013.831438.
28 A. Dsouza, C. Constantinidou, T. N. Arvanitis, D. M. Haddleton, J. Charmet and R. A. Hand, Multifunctional Composite Hydrogels for Bacterial Capture, Growth/Elimination, and Sensing Applications, *ACS Appl. Mater. Interfaces*, 2022, **14**(42), 47323–47344, DOI: 10.1021/acsami.2c08582.
29 D. E. Marx and D. J. Barillo, Silver in Medicine: The Basic Science, *Burns*, 2014, **40**, S9–S18, DOI: 10.1016/j.burns.2014.09.010.
30 I. Khansa, A. R. Schoenbrunner, C. T. Kraft and J. E. Janis, Silver in Wound Care-Friend or Foe?: A Comprehensive Review, *Plast. Reconstr. Surg. Global Open*, 2019, **7**(8), e2390, DOI: 10.1097/GOX.0000000000002390.
31 B. Cao, Y. Zheng, T. Xi, C. Zhang, W. Song, K. Burugapalli, H. Yang and Y. Ma, Concentration-Dependent Cytotoxicity

of Copper Ions on Mouse Fibroblasts in Vitro: Effects of Copper Ion Release from TCu380A vs TCu220C Intra-Uterine Devices, *Biomed. Microdevices*, 2012, **14**(4), 709–720, DOI: 10.1007/s10544-012-9651-x.

32 W. Diao, P. Li, X. Jiang, J. Zhou and S. Yang, Progress in Copper-Based Materials for Wound Healing, *Wound Repair Regen.*, 2024, **32**(3), 314–322, DOI: 10.1111/wrr.13122.

33 M. Claudel, J. V. Schwarte and K. M. Fromm, New Antimicrobial Strategies Based on Metal Complexes, *Chemistry*, 2020, **2**(4), 849–899, DOI: 10.3390/chemistry2040056.

34 B. Sharma, S. Shukla and R. Rattan, *et al.*, Antimicrobial Agents Based on Metal Complexes: Present Situation and Future Prospects, *Int. J. Biomater.*, 2022, **2022**, 6819080, DOI: 10.1155/2022/6819080.

35 M. A. Khalil, G. M. El Maghraby, F. I. Sonbol, N. G. Allam, P. S. Ateya and S. S. Ali, Enhanced Efficacy of Some Antibiotics in Presence of Silver Nanoparticles Against Multidrug Resistant *Pseudomonas aeruginosa* Recovered From Burn Wound Infections, *Front. Microbiol.*, 2021, **12**, 648560, DOI: 10.3389/fmicb.2021.648560.

36 G. Vasiliev, A.-L. Kubo, H. Vija, A. Kahru, D. Bondar, Y. Karpichev and O. Bondarenko, Synergistic Antibacterial Effect of Copper and Silver Nanoparticles and Their Mechanism of Action, *Sci. Rep.*, 2023, **13**(1), 9202, DOI: 10.1038/s41598-023-36460-2.

37 S. Percival, R. Chen and J. A. Hunt Anti-microbial compositions. Published online May 9, 2019. Accessed March 24, 2025. https://patents.google.com/patent/US20190133131A1/en.

38 J. E. Ehlers, N. G. Rondan, L. K. Huynh, H. Pham, M. Marks and T. N. Truong, Theoretical Study on Mechanisms of the Epoxy–Amine Curing Reaction, *Macromolecules*, 2007, **40**(12), 4370–4377, DOI: 10.1021/ma070423m.

39 M. Friedman, Applications of the Ninhydrin Reaction for Analysis of Amino Acids, Peptides, and Proteins to Agricultural and Biomedical Sciences, *J. Agric. Food Chem.*, 2004, **52**(3), 385–406, DOI: 10.1021/jf030490p.

40 J. M. Zatorski, A. N. Montalbine, J. E. Ortiz-Cárdenas and R. R. Pompano, Quantification of fractional and absolute functionalization of gelatin hydrogels by optimized ninhydrin assay and 1H NMR, *Anal. Bioanal. Chem.*, 2020, **412**(24), 6211–6220, DOI: 10.1007/s00216-020-02792-5.

41 A. D. Dias, D. M. Kingsley and D. T. Corr, Recent Advances in Bioprinting and Applications for Biosensing, *Biosensors*, 2014, **4**(2), 111–136, DOI: 10.3390/bios4020111.

42 G. R. Grimsley and C. N. Pace, Spectrophotometric Determination of Protein Concentration, *Curr. Protoc. Protein Sci.*, 2003, **33**(1), 3.1.1–3.1.9, DOI: 10.1002/0471140864.ps0301s33.

43 J. E. Noble Quantification of Protein Concentration Using UV Absorbance and Coomassie Dyes, in *Methods in Enzymology, Laboratory Methods in Enzymology: Protein Part A*, ed. J. Lorsch, Academic Press, 2014, vol. 536, ch. 2, pp. 17–26, DOI: 10.1016/B978-0-12-420070-8.00002-7.

44 F. A. Johnston-Banks Gelatine, in *Food Gels*, ed. P. Harris, Springer, Netherlands, 1990, pp. 233–289, DOI: 10.1007/978-94-009-0755-3_7.

45 E. Magee, F. Xie and S. Farris, *et al.*, Polyelectrolyte Complexation of Chitosan and WS2 Nanotubes, *Adv. Mater. Interfaces*, 2024, **11**(6), 2300501, DOI: 10.1002/admi.202300501.

46 M. J. Swann, N. J. Freeman, F. Watson, S. J. Law and S. L. Percival, A Sensor for Monitoring the Antimicrobial Activity of Wound Dressings for Both Surgical Site Infections (SSIs) and Chronic Wounds, *Surg. Technol. Int.*, 2023, **42**, 65–72, DOI: 10.52198/23.STI.42.WH1692.

47 Y. Xie, C. A. S. Hill, Z. Xiao, H. Militz and C. Mai, Silane coupling agents used for natural fiber/polymer composites: A review, *Composites, Part A*, 2010, **41**(7), 806–819, DOI: 10.1016/j.compositesa.2010.03.005.

48 E. Pulidori, S. Micalizzi and N. Koutsomarkos, *et al.*, Analysis of gelatin secondary structure in gelatin/keratin-based biomaterials, *J. Mol. Struct.*, 2023, **1279**, 134984, DOI: 10.1016/j.molstruc.2023.134984.

49 A. Barth, Infrared spectroscopy of proteins, *Biochim. Biophys. Acta, Bioenerg.*, 2007, **1767**(9), 1073–1101, DOI: 10.1016/j.bbabio.2007.06.004.

50 N. Cebi, M. Z. Durak, O. S. Toker, O. Sagdic and M. Arici, An evaluation of Fourier transforms infrared spectroscopy method for the classification and discrimination of bovine, porcine and fish gelatins, *Food Chem.*, 2016, **190**, 1109–1115, DOI: 10.1016/j.foodchem.2015.06.065.

51 P. Launer and B. Arkles *Infrared Analysis of Organosilicon Compounds*, 2013, pp. 175–178.

52 I. Pucić and T. Jurkin, FTIR assessment of poly(ethylene oxide) irradiated in solid state, melt and aqeuous solution, *Radiat. Phys. Chem.*, 2012, **81**(9), 1426–1429, DOI: 10.1016/j.radphyschem.2011.12.005.

53 S. Padmaja and S. Jayakumar, Functional Group Analysis of CdS:PEO Nanocomposite Solid Films, *Mater. Today: Proc.*, 2018, **5**(6, Part 2), 14473–14480, DOI: 10.1016/j.matpr.2018.03.034.

54 M. Lapointe and B. Barbeau, Understanding the roles and characterizing the intrinsic properties of synthetic *vs.* natural polymers to improve clarification through interparticle Bridging: A review, *Sep. Purif. Technol.*, 2020, **231**, 115893, DOI: 10.1016/j.seppur.2019.115893.

55 J. R. Dias, S. Baptista-Silva and C. M. T. de Oliveira, *et al.*, *In situ* crosslinked electrospun gelatin nanofibers for skin regeneration, *Eur. Polym. J.*, 2017, **95**, 161–173, DOI: 10.1016/j.eurpolymj.2017.08.015.

56 S. Chaibi, D. Benachour, M. Merbah, M. Esperanza Cagiao and F. J. Baltá Calleja, The role of crosslinking on the physical properties of gelatin based films, *Colloid Polym. Sci.*, 2015, **293**(10), 2741–2752, DOI: 10.1007/s00396-015-3660-2.

57 M. K. Yeh, Y. M. Liang, K. M. Cheng, N. T. Dai, C. C. Liu and J. J. Young, A novel cell support membrane for skin tissue engineering: Gelatin film cross-linked with 2-chloro-1-methylpyridinium iodide, *Polymer*, 2011, **52**(4), 996–1003, DOI: 10.1016/j.polymer.2010.10.060.

58 Y. Shirosaki, K. Tsuru and S. Hayakawa, *et al.*, Physical, chemical and in vitro biological profile of chitosan hybrid

membrane as a function of organosiloxane concentration, *Acta Biomater.*, 2009, **5**(1), 346–355, DOI: 10.1016/j.actbio.2008.07.022.

59 M. S. Kim, I. Jun, Y. M. Shin, W. Jang, S. I. Kim and H. Shin, The Development of Genipin-Crosslinked Poly(caprolactone) (PCL)/Gelatin Nanofibers for Tissue Engineering Applications, *Macromol. Biosci.*, 2010, **10**(1), 91–100, DOI: 10.1002/mabi.200900168.

60 H. Lim and S. W. Hoag, Plasticizer Effects on Physical–Mechanical Properties of Solvent Cast Soluplus® Films, *AAPS PharmSciTech*, 2013, **14**(3), 903–910, DOI: 10.1208/s12249-013-9971-z.

61 S. Elderderi, C. Leman-Loubière and L. Wils, *et al.*, ATR-IR spectroscopy for rapid quantification of water content in deep eutectic solvents, *J. Mol. Liq.*, 2020, **311**, 113361, DOI: 10.1016/j.molliq.2020.113361.

62 S. Bashir, M. Hina and J. Iqbal, *et al.*, Fundamental Concepts of Hydrogels: Synthesis, Properties, and Their Applications, *Polymers*, 2020, **12**(11), 2702, DOI: 10.3390/polym12112702.

63 S. Moshayedi, H. Sarpoolaky and A. Khavandi, Fabrication, swelling behavior, and water absorption kinetics of genipin-crosslinked gelatin–chitosan hydrogels, *Polym. Eng. Sci.*, 2021, **61**(12), 3094–3103, DOI: 10.1002/pen.25821.

64 M. Cantini, M. Sousa, D. Moratal, J. F. Mano and M. Salmerón-Sánchez, Non-monotonic cell differentiation pattern on extreme wettability gradients, *Biomater. Sci.*, 2013, **1**(2), 202–212, DOI: 10.1039/c2bm00063f.

65 E. M. Harnett, J. Alderman and T. Wood, The surface energy of various biomaterials coated with adhesion molecules used in cell culture, *Colloids Surf., B*, 2007, **55**(1), 90–97, DOI: 10.1016/j.colsurfb.2006.11.021.

66 Y. P. Yuan, M. R. Hays, P. Hardwidge and J. Kim, Surface characteristics influencing bacterial adhesion to polymeric substrates, *RSC Adv.*, 2017, **7**(23), 14254–14261, DOI: 10.1039/C7RA01571B.

67 S. Zheng, M. Bawazir and A. Dhall, *et al.*, Implication of Surface Properties, Bacterial Motility, and Hydrodynamic Conditions on Bacterial Surface Sensing and Their Initial Adhesion, *Front. Bioeng. Biotechnol.*, 2021, **9**, 643722, DOI: 10.3389/fbioe.2021.643722.

68 P. V. Pulla-Huillca, A. Gomes, A. M. Quinta Barbosa Bittante, R. V. Lourenço and P. J. D. A. Sobral, Wettability of gelatin-based films: The effects of hydrophilic or hydrophobic plasticizers and nanoparticle loads, *J. Food Eng.*, 2021, **297**, 110480, DOI: 10.1016/j.jfoodeng.2021.110480.

69 C. Tonda-Turo, P. Gentile and S. Saracino, *et al.*, Comparative analysis of gelatin scaffolds crosslinked by genipin and silane coupling agent, *Int. J. Biol. Macromol.*, 2011, **49**(4), 700–706, DOI: 10.1016/j.ijbiomac.2011.07.002.

70 J. M. Antosiewicz and D. Shugar, UV-Vis spectroscopy of tyrosine side-groups in studies of protein structure. Part 2: selected applications, *Biophys. Rev.*, 2016, **8**(2), 163–177, DOI: 10.1007/s12551-016-0197-7.

71 G. H. Beaven and E. R. Holiday Ultraviolet Absorption Spectra of Proteins and Amino Acids, in *Advances in Protein Chemistry*, ed. M. L. Anson, K. Bailey and J. T. Edsall, Academic Press, 1952, vol. 7, pp. 319–386, DOI: 10.1016/S0065-3233(08)60022-4.

72 R. Esfandiary and C. R. Middaugh Ultraviolet Absorption Spectroscopy, *Analysis of Aggregates and Particles in Protein Pharmaceuticals*, John Wiley & Sons, Ltd, 2012, pp. 169–200, DOI: 10.1002/9781118150573.ch8.

73 Y. K. Lin and D. C. Liu, Comparison of physical–chemical properties of type I collagen from different species, *Food Chem.*, 2006, **99**(2), 244–251, DOI: 10.1016/j.foodchem.2005.06.053.

74 F. X. Schmid Biological Macromolecules: UV-visible Spectrophotometry, *eLS*, John Wiley & Sons, Ltd, 2001, DOI: 10.1038/npg.els.0003142.

75 D. B. Wetlaufer Ultraviolet spectra Of Proteins and Amino Acids, in *Advances in Protein Chemistry*, ed. C. B. Anfinsen, K. Bailey, M. L. Anson and J. T. Edsall, Academic Press, 1963, vol. 17, pp. 303–390, DOI: 10.1016/S0065-3233(08)60056-X.

76 G. C. Na, UV Spectroscopic Characterization of Type I Collagen, *Collagen Relat. Res.*, 1988, **8**(4), 315–330, DOI: 10.1016/S0174-173X(88)80003-7.

77 F. Yu, K. Prashantha, J. Soulestin, M. F. Lacrampe and P. Krawczak, Plasticized-starch/poly(ethylene oxide) blends prepared by extrusion, *Carbohydr. Polym.*, 2013, **91**(1), 253–261, DOI: 10.1016/j.carbpol.2012.08.008.

78 A. Hashemi Doulabi, H. Mirzadeh, M. Imani and N. Samadi, Chitosan/polyethylene glycol fumarate blend film: Physical and antibacterial properties, *Carbohydr. Polym.*, 2013, **92**(1), 48–56, DOI: 10.1016/j.carbpol.2012.09.002.

79 S. Zivanovic, J. Li, P. M. Davidson and K. Kit, Physical, Mechanical, and Antibacterial Properties of Chitosan/PEO Blend Films, *Biomacromolecules*, 2007, **8**(5), 1505–1510, DOI: 10.1021/bm061140p.

80 H. U. Zaman, J. M. M. Islam, M. A. Khan and R. A. Khan, Physico-mechanical properties of wound dressing material and its biomedical application, *J. Mech. Behav. Biomed. Mater.*, 2011, **4**(7), 1369–1375, DOI: 10.1016/j.jmbbm.2011.05.007.

81 M. Bustamante-Torres, B. Arcentales-Vera, J. Estrella-Nuñez, H. Yánez-Vega and E. Bucio, Antimicrobial Activity of Composites-Based on Biopolymers, *Macromol*, 2022, **2**(3), 258–283, DOI: 10.3390/macromol2030018.

82 M. Georgescu, I. Gheorghe, C. Curutiu, V. Lazar, C. Bleotu and M. C. Chifiriuc, Virulence and resistance features of *Pseudomonas aeruginosa* strains isolated from chronic leg ulcers, *BMC Infect. Dis.*, 2016, **16**(1), 92, DOI: 10.1186/s12879-016-1396-3.

83 S. Shrestha, B. Wang and P. K. Dutta, Commercial Silver-Based Dressings: In Vitro and Clinical Studies in Treatment of Chronic and Burn Wounds, *Antibiotics*, 2024, **13**(9), 910, DOI: 10.3390/antibiotics13090910.